Weather and catchment morphology drive thermal regime variation among sub-Arctic ponds, and possible effects on resident Arctic charr

Grant E. Haines[1]
grant@holar.is
ORCiD: 0000-0001-9085-0022

Joseph S. Phillips[2]
ORCiD: 0000-0003-2016-1306

Elizabeth A. Mittell[3]
ORCiD: 0000-0002-5801-614X

Bjarni K. Kristjánsson[1]
ORCiD: 0000-0001-6984-5771

Camille A.-L. Leblanc[1]
ORCiD: 0000-0003-4861-9948

1 - Hólar University, Dept. of Aquaculture and Fish Biology
2 - Creighton University, Dept. of Biology
3 - University of Edinburgh, Institute of Ecology and Evolution, School of Biological Sciences

ABSTRACT

Thermal stratification, which is a common feature of lentic freshwater systems, has extensive effects on ecological interactions and ecosystem function, including processes that may determine which ponds can support fish populations and affect growth, phenology, and metabolism where populations exist. Because these habitats are important for Northern freshwater fishes, improvement of our ability to forecast thermal stratification and associated ecological processes, like dissolved oxygen dynamics, could increase the accuracy of occupancy and distribution modeling, inform conservation strategies, and predict contemporary evolutionary patterns. Although thermal regimes in temperate systems are well-characterized, the irregular thermal regimes that are often present in small Arctic and subarctic lakes and ponds are more poorly understood. In a unique cave pond system near Mývatn Iceland, where conditions shaped by thermal stratification may be acting as selective agents on divergence of Arctic charr populations, we found differences in thermal stratification regimes related to the orientation of cave openings and the highly irregular catchment topography . In particular, while greater exposure to warm air temperatures can facilitate summer stratification and results in more variable temperatures, exposure to wind – which is modulated on a small scale by the terrain – can facilitate mixing. These patterns caused only the more sheltered of the two ponds remain continuously mixed. We also found that growth rates and body condition in the ponds' Arctic charr populations (*Salvelinus alpinus*) are consistent with constraints on growth and metabolism imposed by low temperature in the cooler, continuously mixed pond, although we cannot rule out the effects of prey limitation.

INTRODUCTION

As major sources of ecological variation between lentic aquatic habitats, the mixing regimes of lakes and ponds can have large and important effects on the ecological processes occurring within them (Boehrer and Schultze 2008; Woolway et al. 2022). Thermal stratification between water layers entails not only gradients of temperature, but also dissolved oxygen (DO), salinity, CO_2, CO_4, and nutrients (Gibson 1999; Song et al. 2013; Rabaey and Cotner 2024). In most lakes wind drives mixing, and most large temperate lakes are dimictic, mixing in the spring and autumn (Boehrer and Schultze 2008). In polar regions, however, where temperatures remain cool in the summer, thermal regimes can be irregular even in large lakes, with some remaining stratified throughout the year (Gibson 1999), stratifying along a chemocline generated by snow- and ice-melt (Cortés and MacIntyre 2020), or exhibiting weak stratification or polymixis. For example, in Iceland, even deep lakes that are dimictic, notably Þingvallavatn (Adalsteinsson et al. 1992; Malmquist et al. 2020) and Lagarfljót (Ramón et al. 2020), are typically weakly stratified and can vary considerably in strength of stratification between years, and can sometimes be thoroughly mixed by strong winds even in the summer (Malmquist et al. 2020). Most lakes and ponds at this latitude, however, are much smaller and/or shallower than these dimictic lakes (Verpoorter et al. 2014), and even in temperate regions, shallow lakes often have more complex mixing regimes. Holgerson et al. (2022) found that ponds in southern Ontario larger than 4 ha were usually isothermal with any stratification breaking down at night. In contrast, ponds with a smaller surface tended to mix intermittently if less than ~74 cm deep, and rarely or never mix if deeper. The extent to which these observations apply to ponds with complex or irregular basin topography, and in cooler subarctic regions where there is typically a smaller difference in the air temperature and the water temperature, is unclear. Such small ponds may have already undergone dramatic community changes with warming climate (Nishikawa et al. 2024), and are important drivers of larger-scale ecological processes (Rautio et al. 2011) across a region that is rapidly warming.

Among the vertebrates that use subarctic ponds and small lakes, the small number of Northern fish species that inhabit them year round is expected to be most directly and acutely affected by variation in thermal regimes. By changing lake and pond thermal regimes, climate change is expected to dramatically alter the suitability of some habitats, forcing populations of these northern species, to migrate or adapt to these changes where migration is not possible (Jeppesen et al. 2020; Kelly et al. 2020). Still, the thermal regimes of their habitats are expected to strongly influence growth patterns, phenology, and population dynamics. For example, although one such broadly distributed species, the Arctic charr (*Salvelinus alpinus*), exhibits extremely high levels of intraspecific diversity and is able to occupy a large range of aquatic habitats, its habitat use is constrained by both temperature and dissolved oxygen concentrations (Elliott and Baroudy 1995; Kelly et al. 2020). Understanding the current interactions between charr populations and the thermal regimes of their habitats is therefore critical for understanding the ecology of these systems, and anticipating future adaptation and local extinction risk.

Temperature and dissolved oxygen are key parameters associated with mixing regimes that affect fish physiology, development, and behavior (McDonald and McMahon 1977; Cote et al. 2020; Rodrigues et al. 2022), which can generate selective pressures, potentially reinforcing reproductive isolation between populations (Ohlberger et al. 2013; Kahilainen et al. 2014). Although Arctic charr are very tolerant of cold water, even to the extent that they can continue to grow at nearly freezing temperatures (Elliott and Baroudy 1995), their phenology and development is heavily influenced by temperature, DO, and their interaction. In hypoxic

conditions, embryo weight and weight at hatching are reduced, and mortality of alevins at relatively warmer temperatures dramatically increases (Gruber and Wieser 1983). Even in cold water, low DO can result in significant alevin mortality, and at 5º, Baroudy (1993) showed that 7-day survival for charr from Windermere, England was 100% at 75% oxygen saturation (9.6 mgL^{-1}), but only 25% at 50% oxygen saturation (6.4 mgL^{-1}). Additionally, temperature variation can constrain spawning phenology (Alekseyev et al. 2019). Slight temperature increases can also increase growth post-hatching (Leblanc et al. 2019), and can strongly influence the development of head morphology, with elevated temperatures resulting in a morphology similar to that seen in benthivorous charr morphs (Hooker et al. 2023). The closely related brook charr (*Salvelinus fontinalis*) even exhibits transgenerational plasticity in which the offspring's expression of genes related to immunity, metabolism, and neural development is affected by the temperatures experienced by parents during gametogenesis (Banousse et al. 2024), which could induce variation between age cohorts and populations in response to thermal regime variation.

We focus our investigation of thermal regimes on groundwater-fed ponds that are situated within lava caves inhabited by distinct small populations of small-bodied Arctic charr in the Mývatn and Laxá Conservation Area in Northeast Iceland (Judson et al. 2024; Leblanc et al. 2024). Environmental microgeographic variation alongside isolation can therefore be expected not only to produce variation in ecological dynamics, but also to facilitate evolutionary divergence over very small spatial scales through selection on behavior, developmental, and physiological processes. Such small-scale divergence has been documented in aquatic habitats spanning lotic-lentic gradients (Haenel et al. 2021), between reproductive habitats of different temperatures (Kavanagh et al. 2010; Arietta and Skelly 2021), and between distinct habitat patches within tidal marshes (Wagner et al. 2017). We also know that invertebrate communities in the cave ponds, on which the charr are dependent for food, are shaped by temperature and dissolved oxygen concentrations (Kristjánsson et al. 2024). Especially for metapopulations with small constituent populations vulnerable to local extinction, such adaptive variation is expected to be critical for enabling adaptation to climate change (Denney et al. 2020; Arietta and Skelly 2021).

To consider whether variation in thermal regimes between ponds could be an important driver of small-scale ecological variation and divergence in Arctic charr, which exhibits particularly high diversity in phenotype (Klemetsen 2013), we analyzed depth profiles for two adjacent cave ponds. Each of the ponds is the habitat for a population of small-bodied Arctic charr, and the two populations experience little gene flow between them (Leblanc et al. 2024). These ponds are partially subterranean and have highly irregular basin and surface morphology that differs between the ponds, but are also inferred to have the same groundwater source and similar water chemistry due to their proximity. Therefore, we hypothesized that the deeper and more sheltered of these two ponds, C24, would stratify and the other, C23, would mix more regularly or continuously (see pond descriptions below). If ponds demonstrated stratification, we modelled meteorological data for potential contributions to the ponds' thermal mixing regimes. The relative contributions to pond stratification of local surface terrain and weather shared across the Mývatn lava fields is important for determining the potential heterogeneity of mixing regimes across the hundreds of ponds in this area, and determining whether temporal variation in thermal regimes is predictable. Because stratification can modulate the suitability of a habitat for charr, we used the stratification models to hindcast thermal dynamics during summers from 2013-2024 to demonstrate its potential utility in reconstructing the environments experienced by charr populations in the ponds. We also tested for associations between changes in stratification

intensity and dissolved oxygen in the summer of 2024 to determine if it is likely that stratification plays a role in modulating DO dynamics. Finally, as divergent thermal regimes are likely to affect Arctic charr body condition and growth patterns, we tested for differences between ponds and sampling seasons in the body conditions of fish captured between 2014 and 2024.

METHODS

Site Description

The ponds described here are located in a lava field directly northwest of the southern basin of Mývatn, a large shallow lake in Northeast Iceland. The lava field contains numerous caves formed by lava tubes, many of which are filled with groundwater that creates permanent ponds. Twenty ponds, in two locations west and northwest of the lake have been the subjects of a long-term monitoring project since 2012 because they contain small populations of small-bodied Arctic charr founded within the past 2200 years, and described in Leblanc et al. (2024).

This study focuses on two cave ponds in particular, hereafter referred to as C23 and C24 (65.61722º N, 17.05426º W and 65.61718º N, 17.05376º W, respectively) which are located 14 m apart. Despite their proximity, they contain Arctic charr populations with low rates of gene flow from C23 to C24, and no detectable gene flow in the other direction (migration rate from C23 to C24 = 0.110 per generation, p = 0.04; Judson et al. 2024; Fst = 0.093; Leblanc et al. 2024). C23 has two openings separated by a low arch approximately 5 m wide, with the passage between them oriented in an east-west direction. A total of 2.2 m^2 of the surface of C23 is exposed to direct overhead sunlight or precipitation and 5.8 m^2 of vertical area separates the surface of the water and the ceiling of the cave at the openings. C24 has one larger opening and an immediately adjacent smaller one, with a combined surface of approximately 2 m^2 or less xposed to the sky. There is only a negligible vertical area at the larger opening of C24 – likely less than 1 m^2 – meaning there is almost no space between the surface of the water and the ceiling of the cave chamber at the opening. The surface of C24 is mostly shielded from wind by turf hummocks. Although we believe most of the pond area of C23 is visible, C24 likely includes a substantial area that is inaccessible not measurable without diving equipment. The substrate of these ponds is predominantly fine organic mud, with some rocky areas near the shore. They lack macrophytes but have attached algae and diatoms that serve as primary producers.

Temperature and Dissolved Oxygen Measurements

We recorded temperature profiles by suspending HOBO data loggers (UA − 002-64 Onset Corporation, Bourne, MA) 20 cm apart along vertical transects from buoys at the deepest accessible points of C23 and C24. Because water levels were unusually high when temperature loggers were deployed due to late snowmelt, suspending them from anchored buoys instead of anchoring the loggers directly allowed them to maintain their depth relative to the surface, but likely resulted in some change in the distance from the benthos (which was <20 cm when deployed). Loggers recorded temperatures in the caves at 6-hour intervals from June 20 to September 4, 2024. Additionally, shoreline temperature loggers have been deployed at C23 and C24, along with the other ponds in the long-term cave charr study. These are not used in the analyses described here, but could be used in future stratification hindcasting models.

We obtained daily average air temperature, wind speed, and wind direction data from Veðurstofa Íslands (the Icelandic Meteorological Office) for the Mývatn weather station (65.61933° N, -16.97684° W, 3.5 km east of the ponds) for the period during which our water

temperature loggers were deployed in C23 and C24. We also collected air temperature data at 6-hour intervals using a HOBO logger deployed at a site approximately 3.68 km south of the ponds (65.58413° N, -17.05642° W) to obtain data on diel fluctuations of air temperature near a cave opening and ensure that temperature data from different locations within the study area were consistent with each other.

Dissolved oxygen (DO) was recorded using a miniDOT logger (PME, Vista, CA) placed near the center of C23, which took measurements at 1-hour intervals from June 21, 2024 – September 18, 2024. This probe was positioned so that it was 18 cm above the bottom, and the temperatures it logged corresponded with the temperatures at 100 cm depth in our depth profile. The logger was removed for 10-30 min on August 21 so that the pond could be electrofished and then replaced at a slightly different location. Although there appears to have been little effect on the measured water temperature, the move of the probe, and mixing and suspension of sediment caused by wading through the pond to electrofish, may have influenced subsequent DO concentrations. As a result, DO data collected following the repositioning of the probe has been omitted from subsequent analyses, but is shown in Figure S1.

Limnological Calculations and Data Analysis

All data processing and analysis was conducted in R v. 4.5.1 (R Core Team 2025). Data from temperature profiles were synchronized to common six-hour intervals using linear interpolation (Gebhardt et al. 2024). We calculated the thermocline depth, when possible, using the *ts.thermo.depth* function in the R package rLakeAnalyzer (Winslow et al. 2019) using the default minimum density gradient cutoff. We calculated Relative Thermal Resistance to Mixing (RTRM; Wetzel 2001; Song et al. 2013) – a metric of water density differential based on temperature – in both caves between the shallowest (20 cm) and deepest (100 cm in C23; 140 cm in C24) HOBO loggers. Because the chemical identities of solutes are unknown in the ponds, and because of the similarity of their water chemistry due to proximity and sharing of a common catchment, RTRM was calculated using densities for pure water.

Although authors sometimes set a threshold RTRM value to define stratification (see e.g., Song et al. 2013), the density or temperature gradient thresholds and related parameters used to define stratification are often unreported, or arbitrary and inconsistent (Gray et al. 2020; Holgerson et al. 2022). Additionally, density gradients in Arctic and subarctic lakes and ponds are often less extreme because the density of water changes more rapidly relative to temperature when it is warmer, and these lakes are typically exposed to cooler summer temperatures than temperature lakes. For instance, Þingvallavatn, Iceland's largest natural lake, is considered to be dimictic, but the temperature gradient at its thermocline is approximately an order of magnitude less than what we measured in C23 (Adalsteinsson et al. 1992; Jónasson 1992). A fixed threshold RTRM value for stratification in this investigation would also be arbitrary, so we refrain from defining one, and instead rely on RTRM values to describe a continuous gradient of stratification.

We tested for the influence of daily average wind direction, wind speed, and air temperature on RTRM as a measure of the extent of stratification in C23, using generalized additive models (GAMs) as implemented in the R package *mgcv* (Wood 2011; Wood 2023). Multiple models were fit with different combinations of predictors and then compared using AIC scores to determine which combination of predictors best explained variation in RTRM. To make the total number of models more manageable, we included main effects of air temperature and wind direction in each model, as these were expected to be the principal drivers of thermal

stratification. Wind speed was only included in some models as a main effect because its influence on RTRM was generally expected to be contingent on wind direction. Model variants were then defined by the inclusion (or lack thereof) of wind speed and interactions (two- and three-way) between air temperature, wind direction, and wind speed. As the response of RTRM to the physical predictors was unlikely to be instantaneous, models were fit using both 1-day and 2-day lags on independent variables, with all terms in a given model lagged in the same way. We then tested a null model with no independent variables. The smoothing splines for wind direction were implemented as cyclic cubic regression splines, and thin plate regression splines used for other variables were unpenalized for main effects and penalized for interactions to minimize excessive wiggliness (Wood 2003, 2017).

While the non-seasonal models have the benefit of being able to predict RTRM using only a single day's meteorological data, their main drawback is that they cannot account for seasonal variation. To account for potential seasonal variation, the best-fitting GAM was refit with a term for "day of the year", fit with a thin plate regression spline (TPRS). The "day of the year" terms captured autocorrelated changes in the fitted values of the model. However, residuals could also be autocorrelated, which has different implications for the other model components are fit to the data. Therefore, we also fit variants of the models accounting for residual autocorrelation. This was done using a first-order autoregressive process using the *corAR1* function in the *nlme* R package (Pinheiro et al. 2023), following procedures described in Simpson (2018) and Enevoldsen et al. (2022) that are further described in the supplementary materials.

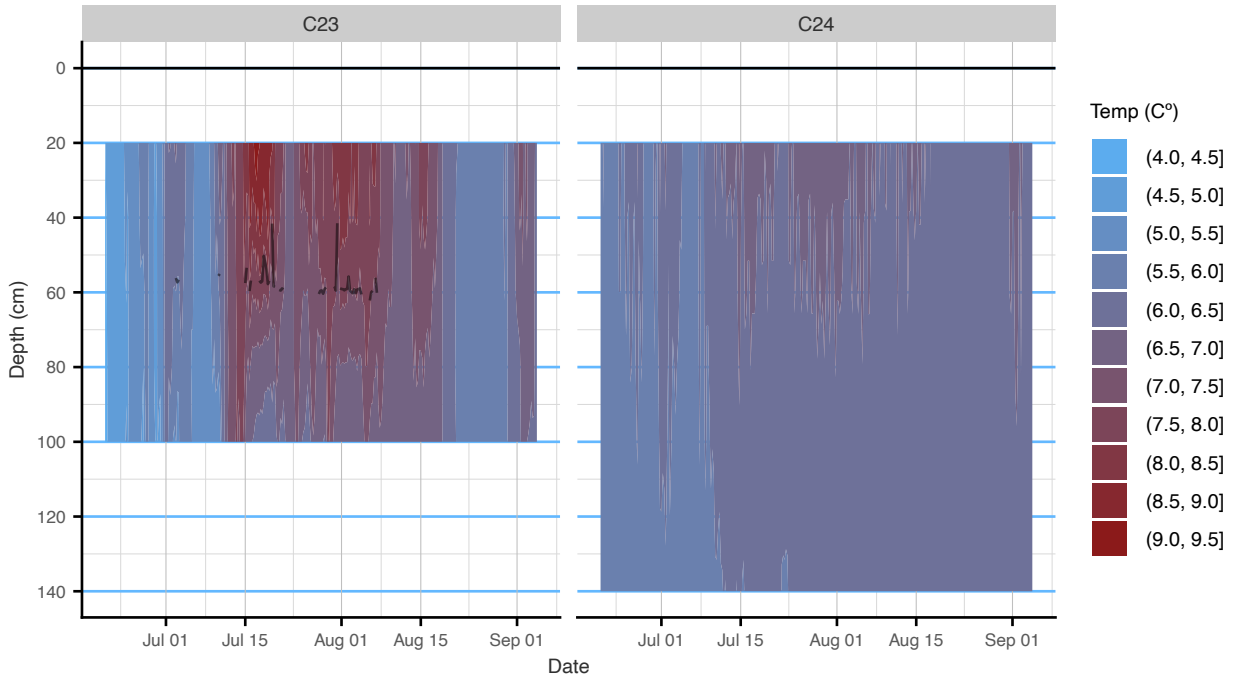

Fig. 1. Temperature profiles in two small groundwater fed ponds (Mývatn, Northeast Iceland) in summer 2024. Temperatures are shown on a color scale from blue to red, representing cooler to warmer temperatures. The thin black line in the C23 profile shows the calculated thermocline depth. The filled area represents the range of depths covered by the temperature data, while the horizontal black line represents the surfaces of the ponds

Because the variance of RTRM increases with its magnitude, all GAMs used a Tweedie distribution with a log-link function. The Tweedie distribution encompasses various continuous and discrete distributions depending on the value of the an estimated parameter p, including the Poisson ($p = 1$) distribution, the gamma ($p=2$) distribution, and mixtures of the two ($1< p <2$) (Dunn and Smyth 2005). This makes it a very flexible way for modeling nonnegative values with potential overdispersion. While negative RTRM values are possible, they are highly transient because they indicate denser water higher in the water column (physically unstable), and they were rarely present in our time series, accounting for only 1 of 74 daily mean RTRM values (-0.034) in the C23 dataset, and approximately 3% of values in the 6-hourly dataset. Therefore, we added the absolute value of the minimum RTRM to all response values, so no values were negative and models could be fitted using the log-link function.

The non-seasonal model with the lowest AICs and its associated seasonal model were then used to hindcast RTRMs of C23 from May 15 – September 30 (inclusive) from 2013 – 2024. If the magnitude of mortality and plastic effects of thermal stratification on the charr populations are able to be determined through continued study of these populations, existing charr data may be used to estimate mortality and selection resulting from yearly variation in stratification dynamics.

Finally, although establishing a mechanistic model of DO variation in these ponds is outside the scope of this paper, we used a rolling correlation of DO and RTRM measured at 6-hr intervals to determine whether a mechanistic association between DO and thermal stratification is likely. Because DO experienced dramatic diel fluctuations from mid-July through the 3rd week of August, DO and RTRM changes relative to the same time on the previous day were used to remove this effect. Correlations used a 3-day (12 time-point) lagging window. DO data following the August 21 removal and replacement of the DO probe are reported in supplementary materials (Figure S1), but were excluded from this analysis because of a subsequent abrupt decline in diel fluctuations that are assumed to be related to the disturbances associated with electrofishing in the pond or probe repositioning.

Charr Length Distributions and Body Condition

To begin to understand the consequences of pond thermal regimes on the resident charr populations, we used phenotypic data collected since 2012 (Leblanc et al. 2024) to test for effects of pond and season on the body conditions of Arctic charr. In most years (excepting when field work was not possible due to inclement weather), data was collected on two occasions at the beginning of the summer growth period in June to early July, and on two occasions near the end of the summer growth period in August to early September. All fish were captured using Gee style minnow traps or electrofishing. Some individuals were observed in two or more sampling periods, but are considered independent for these analyses.

For body condition, we used the Le Cren index (K_n) (Le Cren 1951), with predicted weight-at-length established using common length-mass curve for both populations. While K_n is a ratio of observed to predicted weight that averages to 1 across lengths, the use of a common length-mass curve permits comparisons between populations and seasonal samples, whereas using within-group K_n would place the condition of different groups in non-comparable units (Le Cren 1951; Ghinter and Youcef 2021). K_n was calculated using observations of fish that were at least 45 mm in fork length beginning in the August field season of 2014, when we began using a balance precise to 0.1 grams, whereas our previous balance was only precise to grams. We performed a test for differences between K_n of individuals from different ponds and captured in

different seasons using an ANCOVA that included interactions between fork length and cave or season, and a three-way interaction term, but excluded a term for the main effect of fork length because the use of K_n eliminates that effect. We confirmed the absence of any significant main effect of fork length by running an additional model that included fork length as the first term. Body condition models used type I sums of squares.

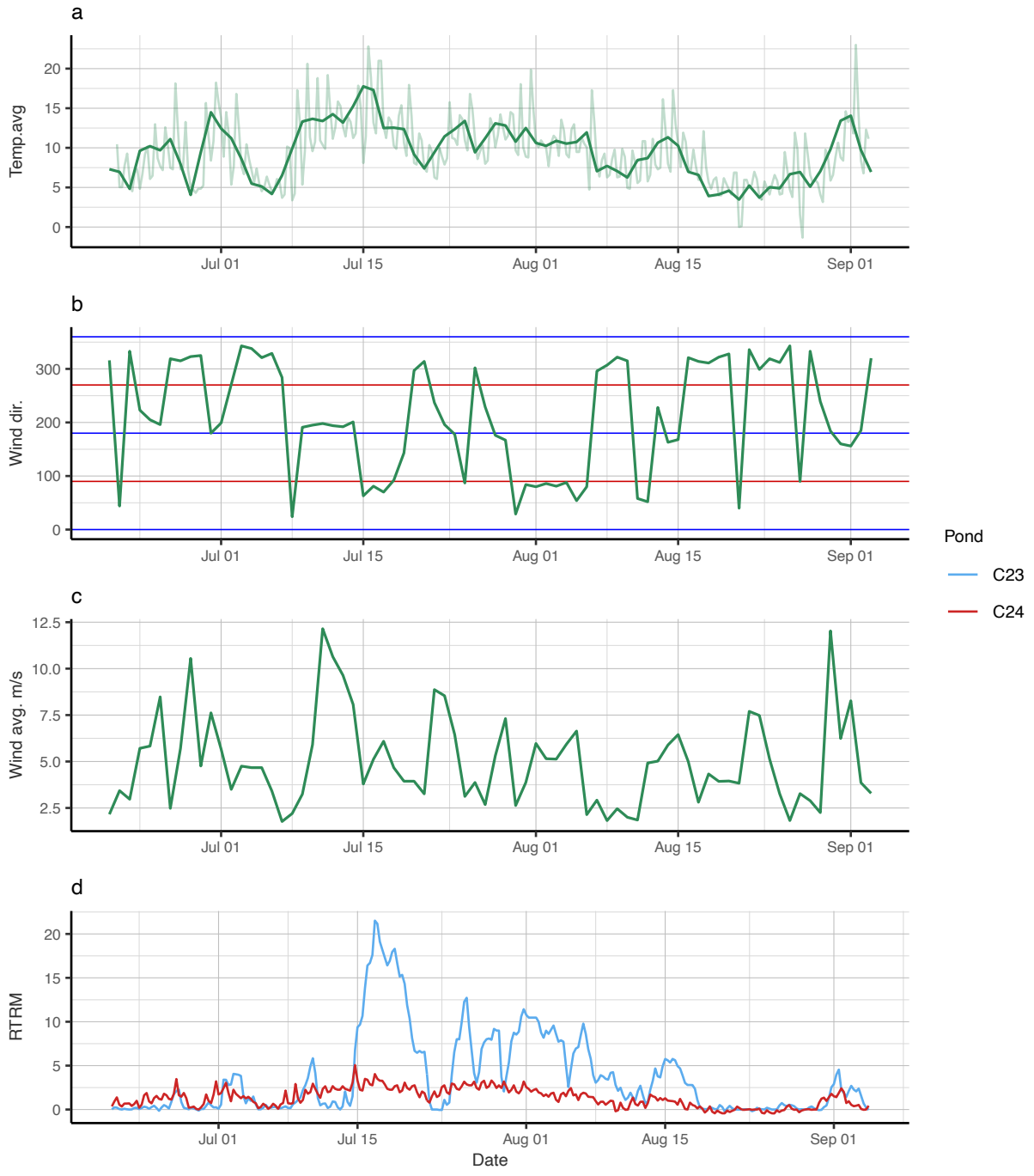

Fig. 2. Local weather conditions and pond stratification dynamics in two small groundwater fed ponds (Mývatn, Northeast Iceland) through summer 2024.
Daily mean temperatures (a), wind direction (b), and wind speed (c) at the 3.5 km distant Mývatn weather station, and Relative Thermal Resistance to Mixing (RTRM) at both caves (d) throughout the study period. The pale green line in

(a) represents air temperature recorded from a HOBO logger at 6-hour intervals 5.28 km southwest of the weather station and 3.68 km south of the ponds, placed near the opening of a pond. This shows that air temperature varies little across the lake, and therefore the weather conditions recorded at the weather station should also be similar to those at the ponds. The diel fluctuations in the logger temperature data are a consequence of the 6-hour sampling resolution. In (b), 0º and 360º represent winds originating from the north. RTRMs of C23 and C24 at 6-hour intervals are shown in (d), with higher RTRM values indicating more intense stratification

Size-specific growth rates are reported from simulated model fits (n = 100 for each pond × season group). Parameters for simulations were extracted from posterior distributions of the "spatial" model in Mittell et al. (2025), which estimated growth coefficients for each population and season, irrespective of year. They used a Bayesian approach to estimate growth rates for 20 populations in the cave ponds around Mývatn, based on repeated observation of tagged individuals.

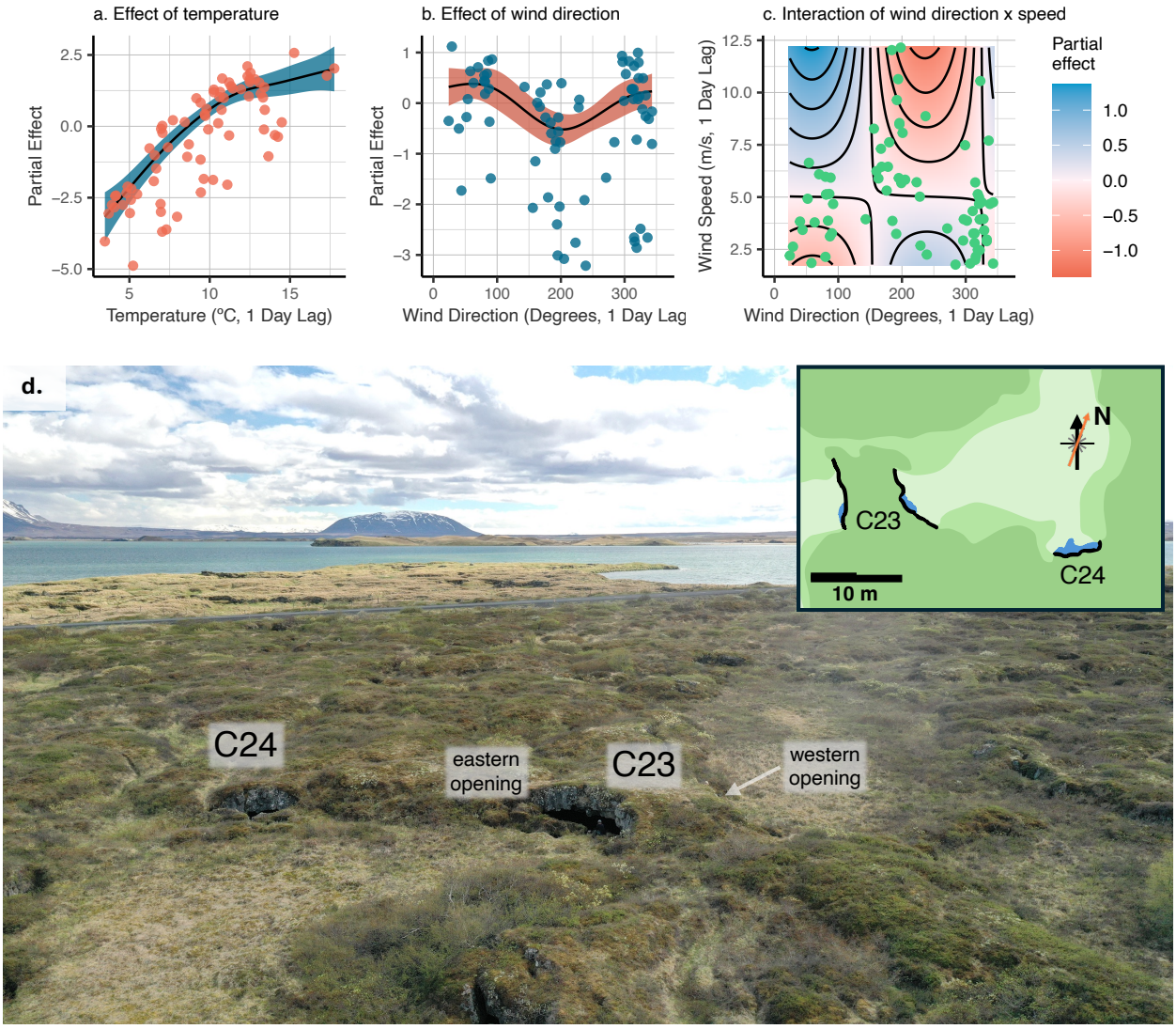

Fig. 3. GAM model 2 partial effects of weather on stratification, and site map and photograph
Partial effects of temperature (a), wind direction (b), and the interaction between wind direction and speed (c) on pond stratification in C23, as measured by Relative Thermal Resistance to Mixing (RTRM) in GAM model 2. Negative partial effects in (a-c) indicate reduced RTRM (increased mixing), while positive effects indicate increased RTRM

(increased stratification). The photograph in (d) shows the study area from the north, facing south, with the south basin of Mývatn in the distance. In the inset map, black lines indicate the cave openings and shading indicates elevation and vegetation type. Pale green indicates grassy areas only slightly above the water table, while the darker greens indicate elevated areas with mostly low, shrublike vegetation. The orange arrow is oriented from 200° SSW, the approximate direction in which wind has the strongest negative effect on stratification. Photo by Kári Heiðar Árnason

RESULTS

Thermal Gradient Formation

Throughout the study period, C24 did not stratify and temperature varied little (Figure 1, S2). The difference between temperatures recorded at 20 cm and 140 cm reached a maximum of 1.0ºC, but rarely exceeded 0.5ºC irrespective of air temperature, and had maximum and median RTRM values of 5.06 and 1.89, respectively, indicating constant, thorough mixing. In contrast, loggers in C23 recorded several distinct periods of elevated RTRM values between mid-July and mid-August, the most prominent of which began on July 14 and lasted for approximately a week (Figure 2). C23 had a maximum temperature difference of 3.0º C between depths of 20 cm and 100 cm, and a maximum RTRM of 21.52 on the afternoon of July 16.

As might be expected for such a shallow pond, when a putative thermocline developed in C23, it was unstable and short-lived. After calculated thermocline depths of exactly 30 and 90 cm – which were assumed to be calculation artefacts – were removed, the most durable thermocline persisted for 4 days, from 18:00 on July 31 to 12:00 on Aug 4. Furthermore, as C23 became more stratified the temperatures recorded by the deeper loggers would decline, becoming colder than when the water column was thoroughly mixed, even as water temperatures near the surface increased (Figure S2).

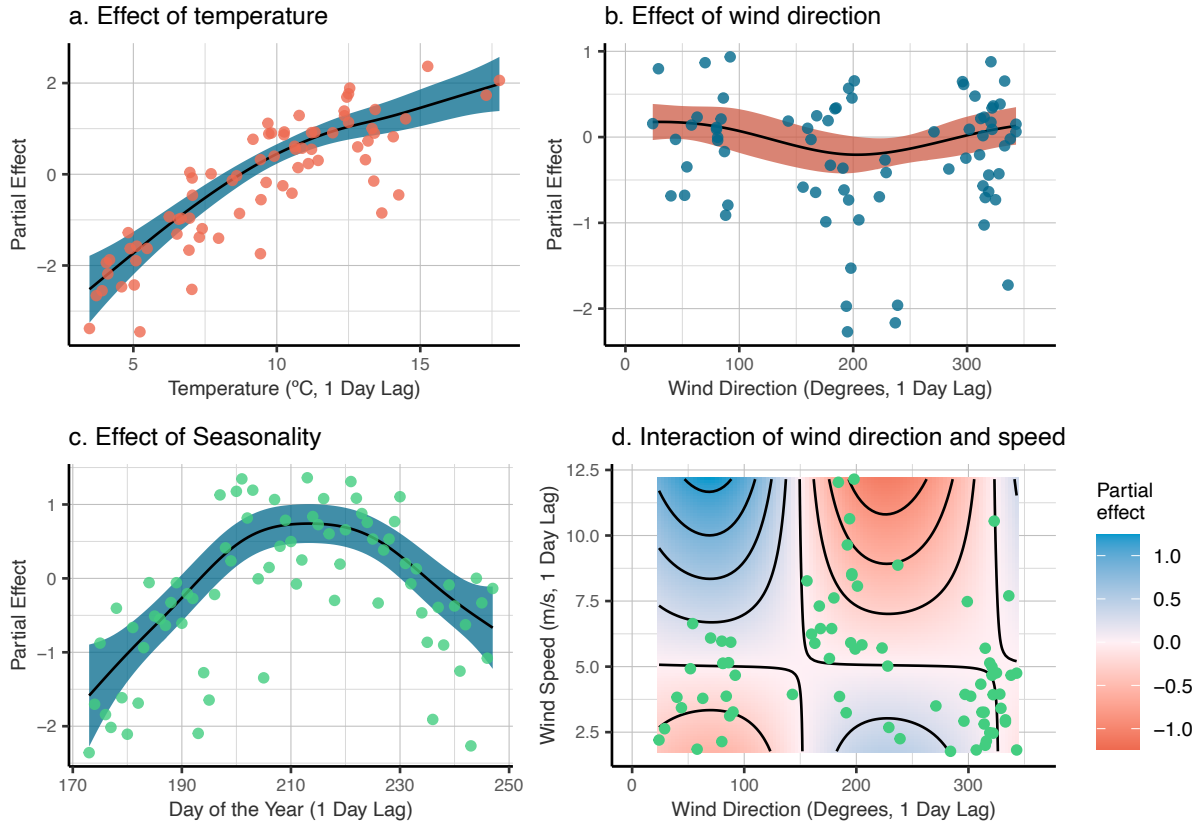

Fig. 4. Partial Effects of weather variables on stratification in Seasonal GAM model
Partial effects of temperature (a), wind direction (b), seasonality (c), and a wind direction × speed interaction (d) in the Seasonal GAM. All effects included in this model are statistically significant. Note that at higher wind speeds, winds from SSW had a negative, de-stratifying effect

Predictors of RTRM

GAMs with 1-day lags on meteorological variables yielded better fits than those with 2-day lags (Table 1). Moreover, the model with 1-day lagged effects of temperature, wind direction, and wind direction × wind speed interaction (Model 2) had the lowest AIC among those models only including meteorological predictors. This model did not include a main effect of wind speed, and fit slightly better than Model 3, which was identical to Model 2 except for its inclusion of a wind speed main effect. Model 2 explained 69.3% of the deviance in RTRM, and each of its terms was statistically significant (Table 2, Figure 3). RTRM increased (i.e., lower mixing) with temperature until approximately 12ºC where the effect of temperature plateaued. Conversely, wind was associated with reduced RTRM (i.e., greater mixing) when coming from approximately 200º SSW, corresponding to more direct exposure to the western opening of C23 (Figure 3). In Model 2, greater wind speed promoted greater mixing, but only when it aligned with wind directions of greatest exposure, as indicated by the wind direction × wind speed interaction (Figure 3).

The addition of the seasonal component ("day of the year") to Model 2 substantially improved the model fit and raised the deviance explained to 84.9%. However, the inferred effects of temperature, wind direction, and wind direction × wind speed interaction as described above were largely unchanged directionally, although the main effect of wind direction was somewhat weaker. RTRM showed a hump-shaped relationship with day of the year, with a peak in late July ("day of year" 210; Figure 4). This pattern ostensibly cannot be directly explained by air temperature (as this was separately accounted for in the model) but could be tied to a related mechanism that manifests over a different time scale. Accounting for residual autocorrelation further improved the fit of the model in terms of AIC, but reduced the deviance explained by the predicted values under the model (i.e., excluding the residuals) to about 76.1%. In this model, the effects of temperature, wind direction, and seasonal smooth were significant (Table 2); but those effects were weaker than for the models omitting the residual autocorrelation structure (Figures S3-S4), and the effect of wind direction was so weak as to not be practically meaningful. Moreover, the wind direction × wind speed interaction was not significant. Essentially, the model including a residual autocorrelation structure attributed a greater portion of the autocorrelated variation in RTRM data to residual error, reducing the influence of the predictors. While mathematically clear, there is some mechanistic ambiguity in the attribution of observed temporal autocorrelation to the predicted values (i.e., meteorological predictors; seasonal smooth) versus error (i.e., residual autocorrelation). As our goal was to understand the potential influence of the model predictors, we hereafter focus on the results from the model including the meteorological predictors and seasonal smooth, but not residual autocorrelation.

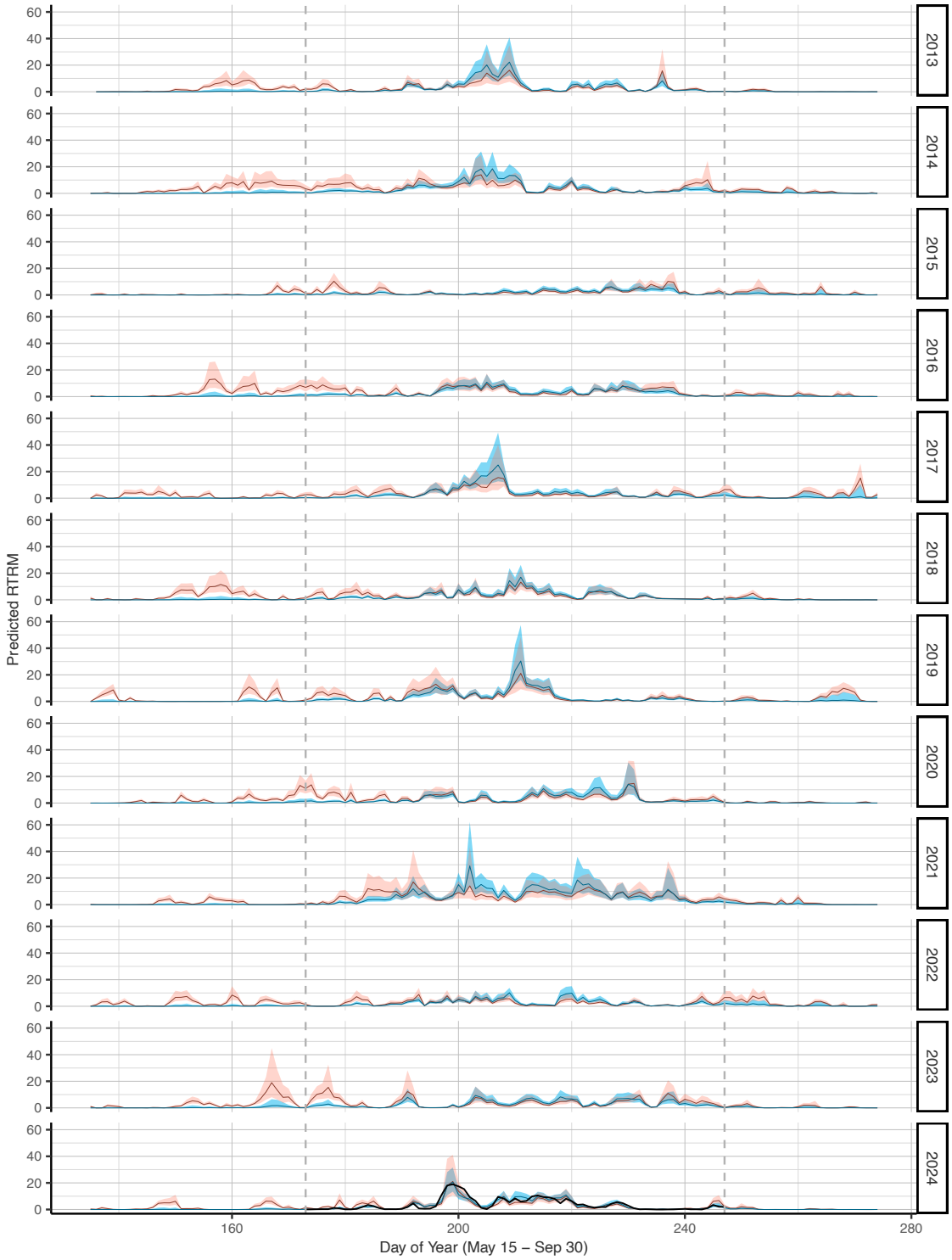

Fig 5. Hindcasted stratification in a small pond in Northeast Iceland from local meterological data for 2013-2024 Daily mean Relative Thermal Resistance to Mixing (RTRM) in C23, empirically calculated (black; 2024 only) and hindcasted RTRM from GAM Model 2 (blue) and the Seasonal Model (red), with 95% credible intervals shaded. Vertical dashed lines represent the beginning and end of the date range of empirical stratification data used in the models. Both models included main effects of temperature and wind direction and a wind direction × wind speed interaction, all on a 1-day lag. The seasonal model additionally had a term for the day of the year.

To characterize the expected mixing regime under different meteorological conditions, we hindcasted the model using temperature, wind speed, and wind direction data from May 15th to September 30th of every year from 2013 to 2024. For the sake of comparison, we did this for both the model including a seasonal smooth and without, with the caveat that the seasonal smooth was only fit to data from June 21 to September 18, 2024 and therefore our hindcasting extended beyond the temporal range of the RTRM data used to fit the model. Nearly every year experienced multiple transient periods of elevated resistance to mixing, although the timing varied substantially across years, and models diverged beyond the dates for which RTRM was calculated in 2024 (Figure 5). Nonetheless, this illustrates that the complex mixing regime observed in 2024 is likely representative of the typical behavior. Inclusion of the seasonal smooth led to lower back-casted RTRM values early and late summer, leading to greater periods of complete mixing than expected based on the meteorological predictors alone.

Dissolved Oxygen

For most of the study period, 24h-changes in RTRM and DO were negatively correlated such that reduced mixing (higher RTRM) was associated with declines in DO (Figure 6). However, this negative association weakened and briefly reversed following the period of strongest stratification in July, became re-established for approximately a week, then again reversed during the weaker stratification at the beginning of August. The correlation coefficient between daily changes in DO and RTRM then gradually declined through mid-August.

Table 1. Model fit summaries for GAM models of effects on stratification

Brief descriptions of all tested general additive models of pond thermal gradient for C23. Model terms are: T – temperature, W_d – wind direction in degrees, W_s – wind speed, D – day of the year. Model 2, the best-fitting non-seasonal model, was used as the basis for the seasonal models. Bold typeface is used to indicate the best-fitting model by Akaike's Information Criterion (AIC) and its seasonal version. Models with a lag of 1 day on independent variables have an *n* of 75, whereas models with a lag of 2 days have an *n* of 74. *P* indicates the *p* parameter of the Tweedie distribution used by *mgcv* to fit the model, not the significance of the model fit

Model No.	Formula	Lag (days)	df	AIC	*p*
Null	~ 1	NA	2	444.1	NA
1	~ T + W_d	1	11.37	273.87	1.721
2	**~ T + W_d + W_dW_s**	**1**	**11.79**	**268.87**	**1.700**
3	~ T + W_d + W_s + W_dW_s	1	13.12	269.55	1.706
4	~ T + W_d + W_s + TW_dW_s	1	12.63	273.15	1.706
5	~ T + W_d + TW_dW_s	1	10.20	272.11	1.725
6	~ T + W_d + W_s + W_dW_s + TW_dW_s	1	15.95	271.56	1.705
7	~ T + W_d	2	8.27	286.67	1.738
8	~ T + W_d + W_dW_s	2	11.69	287.23	1.734
9	~ T + W_d + W_s + W_dW_s	2	12.32	288.28	1.736
10	~ T + W_d + W_s + TW_dW_s	2	9.98	284.81	1.744
11	~ T + W_d + TW_dW_s	2	9.54	283.78	1.740
12	~ T + W_d + W_s + W_dW_s + TW_dW_s	2	11.98	285.78	1.743
Seasonal	**~ T + W_d + W_dW_s + D**	**1**	**15.89**	**224.96**	**1.556**

Table 2. Stratification GAM model results for the best-performing model, with and without a seasonal term and an autoregressive component

Summary results for models 2 and the seasonal model. All GAMs were run using the Tweedie distribution with a log link function. The seasonal model incorporates a Day term, while model 2 requires only the weather data from the previous day. Thin plate regression splines are indicated by TPRS. The wind direction splines are cyclic such that values of 0 and 360 are equivalent. Models 2 – AR1 and Seasonal – AR1 incorporate first-order autoregressive components with values of autocorrelation coefficient ρ reported (see supplementary materials for more on how this value was obtained). Reported REML scores for these two models are fREML scores

Model	Terms	Spline/ Smooth Type	edf	F	P	
2	T	TPRS	3.17	25.03	< 0.001	***
	W_d	Cyclic	2.00	4.60	< 0.001	***
	W_dW_s	Cyclic:TPRS	1.93	0.81	0.004	**
Seasonal	D	TPRS	3.89	15.42	< 0.001	***
	T	TPRS	3.00	23.51	< 0.001	***
	W_d	Cyclic	1.32	1.51	0.0243	*
	W_dW_s	Cyclic:TPRS	2.13	1.31	< 0.001	***
2 – AR1	T	TPRS	2.41	10.29	< 0.001	***
	W_d	Cyclic	0.45	0.17	0.299	
	W_dW_s	Cyclic:TPRS	0.39	0.04	0.271	
	corAR1(~ D)	ρ = 0.83072				
Seasonal – AR1	D	TPRS	3.33	6.74	< 0.001	***
	T	TPRS	2.37	13.46	< 0.001	***
	W_d	Cyclic	0.00	0.00	0.013	*
	W_dW_s	Cyclic:TPRS	0.85	0.11	0.206	
	corAR1(~ D)	ρ = 0.5926354				

	Deviance Explained (%)	DF	AIC	-REML	Scale Estimate
2	69.3	11.79	268.87	134.94	0.730
Seasonal	84.9	15.89	224.96	114.70	0.435
2 – AR1	39.8	7.63	228.89	81.47	1.173
Seasonal – AR1	76.1	11.54	217.04	81.99	0.552

Charr Body Condition and Size-Specific Growth

Both populations exhibited significant differences in body condition between seasons (Table 3, Figure 7), with higher condition in August than June, consistent with increased food availability in the summer. Although there was no difference in the main effect of population on body condition, there was a significant interaction between fork length and population, such that smaller individuals in C24 were heavier than C23 fish of the same length, and the inverse was true for larger individuals. The three-way interaction between population, season, and length was not significant, but the population-specific length effect is particularly prominent in August, with the differences in condition between caves being greater at the end of the growing season (Figure 7). Despite the significant effects, the model had low explanatory power, with an adj. R^2 of only 0.027. Although the Shapiro-Wilk test identified significant departure from normality in the model residuals ($W = 0.956$, $p < 0.001$), this is primarily a consequence of the distribution's light tails, as the positive skew is mild (0.743).

In both ponds, growth was higher in the summer than in the winter months (Table 4, Figure 7). Additionally, growth rates decreased with size in both ponds and across summer and winter seasons. Among larger fish, C23 exhibited higher growth rates in summer and winter, but rates of growth were faster among fish less than ~85 cm in C24 than among similarly-sized fish in C23 during the winter.

Table 3. Effects of sampling season and pond on charr condition

Results of an Ancova for differences in Le Cren Indices between ponds and between seasons. Type I sums of squares are used for this test, and terms are listed in order of inclusion in the model. Lengths were centered about the mean length prior to performing this analysis.

Effect	Df	SS	MS	F	p	
Season	1	0.125	0.125	8.069	0.005	**
Pond	1	0.003	0.003	0.190	0.663	
Season:Length	2	0.073	0.037	2.377	0.094	
Pond:Length	1	0.113	0.113	7.291	0.007	**
Season:Pond:Length	1	0.041	0.041	2.675	0.102	
Residuals	613	9.472	0.015			

Table 4. Trends in size-specific growth rates of charr by pond and season

Seasonal growth rates in mm/month, as a function of fork length. Intercepts represent the value at 93 mm, the mean fork length of individuals in the Mittell et al. (2025) growth models. Slopes represent change in mm/month as a function of fork length.

Pond	Season	Intercept	Intercept 95% CI	Slope	Slope 95% CI
C24	Summer	3.39	3.27, 3.52	-0.0481	-0.0509, -0.0453
C24	Winter	0.78	0.74, 0.83	-0.0169	-0.0175, -0.0162
C23	Summer	3.72	3.59, 3.85	-0.0402	-0.0431, -0.0374
C23	Winter	0.79	0.75, 0.83	-0.0120	-0.0126, -0.0114

DISCUSSION

Here we demonstrated that the catchment morphology and orientation of two subarctic ponds (separated by only 14 m) interacted with local weather conditions and resulted in divergent thermal regimes, providing distinct summer conditions for two populations of Arctic charr. Such small-scale environmental heterogeneity in temperature and DO can have consequences for the species and populations that inhabit these environments. While one cave (C24) remained well-mixed throughout the study period, the other (C23) experienced transient periods of elevated thermal resistance to mixing associated with pronounced thermal gradients. Wind direction played a key role in shaping the mixing regime, with well-mixed periods associated with winds approximately matching the orientation of C23 between openings. Temporal variation in mixing was associated with the DO dynamics, with periods of reduced mixing being associated with declines in DO, presumably due to reduced gas exchange between the atmosphere and the hypolimnion (Smith and Bella 1973). Moreover, although we cannot establish a causal link with thermal regime from the available data, populations of Arctic charr in the two caves differed in their interactions between pond and length to affect body condition and size-specific growth rates. Because temperature and DO influence charr phenology (Alekseyev et al. 2019), growth (Leblanc et al. 2019), survival (Gruber and Wieser 1983; Baroudy 1993; Baroudy and Elliot 1994), and morphology (Hooker et al. 2023), and can restrict the livable volume of a body of water (Smith and Bella 1973), our results suggest that the variation in pond thermal regimes induced by the interaction between weather and wind exposure may play an important role in shaping population ecology at a very fine scale.

Interestingly, distinct differences were found between two ponds that are superficially similar in many respects. Both ponds are largely sheltered from sunlight, share groundwater

origin based on temporal series of chemical parameters (pers. comm. Leblanc), and have relatively small volumes. While the RTRM values calculated in C23 are lower than what is typical for stratified temperate lakes and ponds because of its low year-round temperatures, both C23 and C24 are largely sheltered from most of the disturbances that would induce mixing in more typical ponds because of the lava ceiling and surrounding terrain. Both have very small areas exposed to direct sunlight, meaning that radiative heating of the benthos is not a factor that would induce mixing, and both are generally sheltered from wind, except when the wind direction matches the direction of the cave opening (see Figure 3). Even though C23 has a larger surface exposed to the air, the air temperature in the chamber under the arch is often cooler than the outside air temperature (personal observation). As a consequence, even a relatively low thermal gradient appears able to resist mixing in C23 for days to weeks, except when southwesterly winds are able to force air to flow under the arch and interact with the surface of the pond. Alongside less wind exposure, C24 has a much smaller surface capable of interacting with the air, particularly relative to its possibly large subterranean volume. This likely prevented sufficient warming of its surface to induce stratification in the first place.

The distinct populations of Arctic charr inhabiting these two subarctic ponds exhibited differences in growth rates and condition, which suggests that the local environmental heterogeneity found could be important for these populations. Larger individuals tended to have lower body condition in C24 than similarly-sized individuals in C23 (Figure 7), and the size-dependent growth rate during the winter decreased with body size more slowly in C23 than it did in C24. These patterns are consistent with the tendency of charr and trout to gain mass at rates that increase with temperature in populations along thermal gradients (Murdoch et al. 2015; O'Gorman et al. 2016). However, they might also be a consequence of the restricted access to allochthonous prey inputs in C24, particularly chironomid midges, which are ecologically important species in the Mývatn ecosystem (Einarsson et al. 2004) and make up a large proportion of charr prey in some nearby ponds during the high-growth summer months (Kristjánsson et al. 2012). Pulses in prey availability and thermal regimes may also interact. For instance, Armstrong et al. (2010) showed that the effects of temperature on phenology and growth limit access to prey that is only available to individuals above a certain size threshold. Disentangling these effects will require further work, including data from other stratifying and non-stratifying sites.

The lava fields around Mývatn include hundreds of ponds inhabited by numerous small populations of Arctic charr (Leblanc et al. 2024) and stickleback (Seymour et al. 2013), with varying levels of physical connectedness and gene flow between ponds. While both of the ponds we studied here are very small, and support populations of only a few dozen adult charr (census N: C23 = 60, C24 = 42; N_e: C23 = 6, C24 = 22; Leblanc et al. 2024), all the cave ponds in the lava field of Mývatn may consist of thousands or tens of thousands of individuals. Additionally, many of the caves are irregularly shaped, and often have several distinct basins and openings with varying orientations and degrees of exposure to fluctuations in air temperature, snow accumulation in the winter, and changes in wind speed and orientation. As a consequence, the morphological variation among cave catchments may drive ecological dynamics in this broader system in much more complex ways than the methods employed in the present study would allow us to predict. Nevertheless, this study establishes the importance of the link between the physical surroundings, internal ecological dynamics, and potentially the biotic communities of ponds in close proximity that were previously thought to be environmentally similar and relatively static.

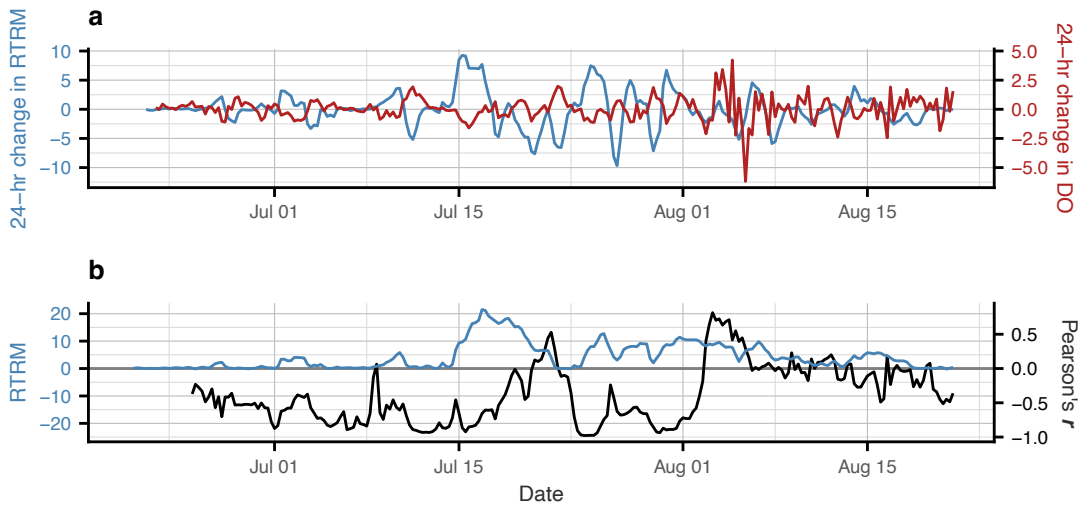

Fig. 6. Stratification and dissolved oxygen dynamics, and their relationship, in a thermally dynamic pond 24-hr change in RTRM (blue) and DO (red) throughout the temperature profile logger deployment is shown in (a). A rolling correlation between daily changes in DO and thermal gradient intensity (Pearson's *r*; black), with a lagging 12-point, 36-hr window, are shown in (b), along with RTRM. Daily changes in RTRM and DO are strongly negatively correlated for most of the period from the beginning of the study to early-August, when the correlation abruptly reverses, then collapses

Limitations

Local environmental heterogeneity and associated phenotypic variation can be difficult to quantify, due to the large sample sizes required to obtain power to statistically support the small effect sizes that are expected. Quantifying how local environmental variation might shape phenotypic variation on a finer scale is of great interest to ecologists and evolutionary biologists, and we have shown that this study system may be especially well suited to to address this subject. However, although there are numerous ponds of varying morphology across the lava fields around Mývatn, this study only included two with relatively simple morphology compared to some more complex, deeper and wider ponds in the area. Some ponds include multiple basins that are deep enough to stratify and have a broad range of vertical openings (i.e. from very low to high lava ceiling above the water surface), meaning less or more direct interaction with the climatic conditions that induce both stratification and mixing. It is therefore unclear how prevalent thermal stratification is in ponds across this landscape, and how important its effects are to the ponds' ecology. These factors make the task of predicting the thermal dynamics in some ponds especially complex.

We have also not directly considered groundwater temperatures or flows in our models of stratification. The flow of groundwater where the two caves are situated is in an approximately south-westerly direction, and is likely responsible for maintaining cool water temperatures in the ponds during summer and preventing them from freezing from top to bottom in the winter. However, the rate of flow and baseline temperature of the groundwater entering the ponds is not known, and without direct measurements, we cannot confirm this stabilizing effect. In addition, because large portions of these ponds are underground, some common limnological variables are not easily measurable, e.g. volume of water, so our models were designed with easily accessible

meteorological data. Similar models for small ponds may be improved with the incorporation of more limnological data.

Finally, because water is densest at 4°C, ponds can be warm- or cold-stratified, and RTRM has positive values during both warm- and cold-stratification. Indeed, in both February 2023 and March 2025, we have observed that the surface of C24 was ice-free while C23 was frozen over, indicating possible annual cryostratification in the latter. However, because our temperature data were collected in the summer, only four days in our dataset had average air temperatures < 4°C, and none of those reached 3°C or below. As a consequence, our models show only a positive effect of temperature on stratification, even though this relationship should reverse as temperatures cross and extend below the 4°C line. This means that the current model fit should not be used to predict RTRM during cooler times of the year, although ongoing data collection should make this possible in the future.

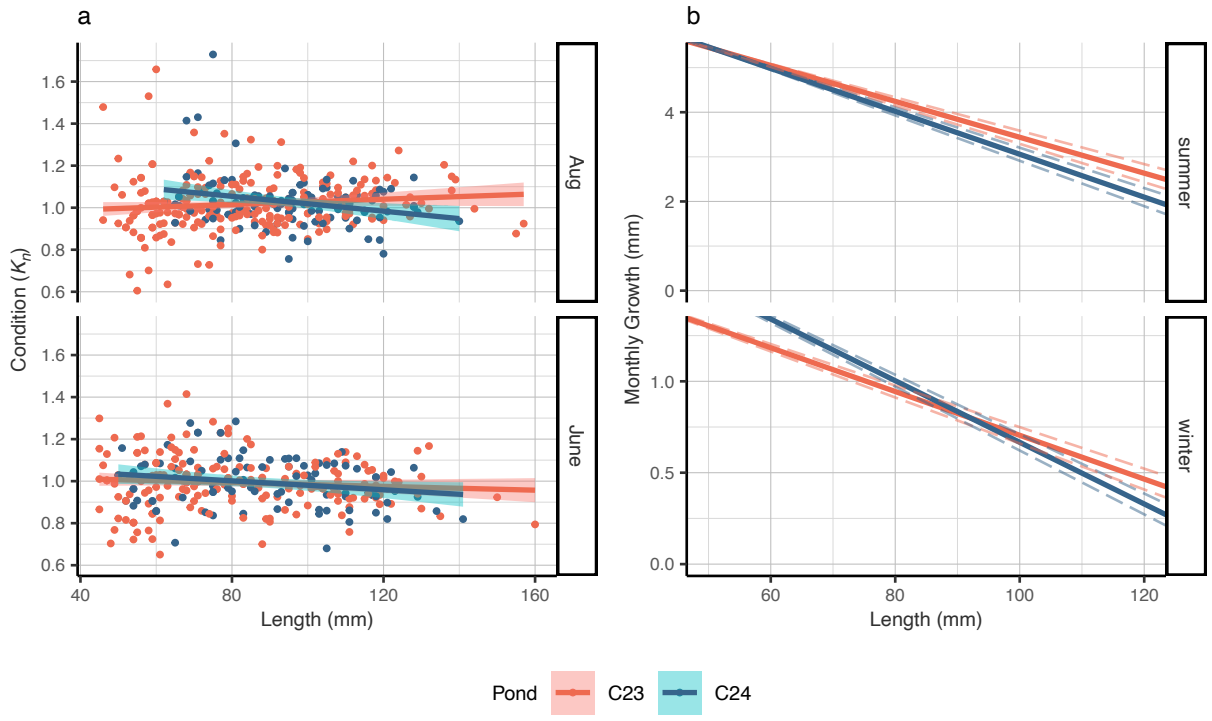

Fig. 7. Body condition and size-specific growth rates in charr populations
Body condition (a) and size-specific growth rates (b) with confidence intervals based on simulated data (n = 100 per group) using the estimated parameters shown in Table 4 (b) of charr in C23 and C24, both ± 95% CI. Reported lengths are fork lengths, and only individuals with fork lengths ≥ 45 mm were included in K_n calculations. Late-summer body condition and winter growth rates are both higher in small individuals and lower in large individuals from C24, compared to similarly-sized individuals from C23. Simulations are based on model parameters from Mittell et al. (2025)

Conclusion

The ponds surrounding Mývatn are of particularly complex morphology due to the recent volcanic history of the region (Thórarinsson 1979), which can result in divergent pond mixing patterns, even over very short distances. The Arctic charr that inhabit these subarctic ponds exhibit differences in growth rates and body condition that could be a consequence of this limnological variation, and similar or related effects are likely to be a common feature of small

populations in freshwater. These effects require further investigation to establish a definitive causal link, and to determine their ecological importance in regulating communities and populations. If such investigations establish strong effects, these dynamics may drive variation across northern aquatic communities and populations across Arctic and subarctic freshwater systems, and be an engine of adaptation in the face of climate change. In a similar localized system, for instance, Gallagher and Fraser (2024) have shown that hatching and emergence phenology in stream populations of brook trout (*Salvelinus fontinalis*) have shifted in response to climate change since 1980, but have changed the least in streams fed primarily by groundwater (which are cooler in the summer and warmer in the winter). Adaptive evolution over contemporary time-scales is a common feature of wild populations (Sanderson et al. 2021), and across Arctic and subarctic environments, lakes and ponds are expected to stratify more frequently and for longer durations as the climate warms (Woolway et al. 2021). The ranges of coldwater fish populations are expected to shift as a consequence (Gillis et al. 2024), forcing populations to either adapt, migrate northward, or face local extinction, and the ability to predict ecological processes, particularly those associated with thermal dynamics, is required to understand the shape these responses will take.

Acknowledgements
We wish to thank Alison Derry for providing comments on an early version of this manuscript. We also thank Kári H. Árnason, Anthony R. Ives, and Emily Adler for their support in the field, as well as Sjoerd Dankers and Bart van der Zande for field assistance. Rannís (grant 228720-051) provided funding support for this project, and we would also like to thank Creighton University for providing funds to JSP for travel costs and field equipment. Meteorological data were obtained from Veðurstofa Íslands (the Icelandic Meteorological Office) on December 4, 2024.

References

Adalsteinsson H, Jónasson PM, Rist S (1992) Physical characteristics of Thingvallavatn, Iceland. Oikos 64:121-135. https://doi.org/10.2307/3545048

Alekseyev SS, Pichugin MY, Gordeeva NV, Samusenok VP, Yur'ev AL, Khlystov VS, Matveev AN (2019) Reproductive strategies and the origin of parapatric and sympatric forms of Arctic charr *Salvelinus alpinus* (Salmonidae) in the system of Lakes Bol'shoe Leprindo and Maloe Leprindo (Northern Transbaikalia). J Ichthyol/Vopr Ikhtiol 59:527-544. https://doi.org/10.1134/S0032945219040015

Arietta AZA Skelly DK (2021) Rapid microgeographic evolution in response to climate change. Evolution 75:2930-2943. https://doi.org/10.1111/evo.14350

Armstrong JB, Schindler DE, Omori KL, Ruff CP, Quinn TP (2010) Thermal heterogeneity mediates the effects of pulsed subsidies across a landscape. Ecology 91:1445-1454. https://doi.org/10.1890/09-0790.1

Banousse G, Normandeau E, Semeniuk C, Bernatchez L, Audet C (2024) Parental thermal environment controls the offspring phenotype in Brook charr (*Salvelinus fontinalis*): insights from a transcriptomic study. G3 14:jkae051. https://doi.org/10.1093/g3journal/jkae051

Baroudy E (1993) Some factors affecting survival and distribution of Arctic charr (*Salvelinus alpinus* (L.)) in Windermere Department of Biological Sciences. University of Lancaster, Lancaster, UK.

Baroudy E Elliot JM (1994) Tolerance of parr of Arctic charr, Salvelinus alpinus, to reduced dissolved oxygen concentrations. J Fish Biol 44:736-738. https://doi.org/10.1111/j.1095-8649.1994.tb01250.x

Boehrer B Schultze M (2008) Stratification of lakes. Rev Geophys 46:RG2005. https://doi.org/10.1029/2006RG000210

Cortés A MacIntyre S (2020) Mixing processes in small arctic lakes during spring. Limnol Oceanogr 65:260-288. https://doi.org/10.1002/lno.11296
Cote D, Tibble B, Curry RA, Peake S, Adams BK, Clarke KD, Perry R (2020) Seasonal and diel patterns in activity and habitat use by brook trout (*Salvelinus fontinalis*) in a small Newfoundland lake. Environ Biol Fishes 103:31-47. https://doi.org/10.1007/s10641-019-00931-1
Denney DA, Jameel MI, Bemmels JB, Rochford ME, Anderson JT (2020) Small spaces, big impacts: contributions of micro-environmental variation to population persistence under climate change. AoB PLANTS 12:plaa005. https://doi.org/10.1093/aobpla/plaa005
Dunn PK Smyth GK (2005) Series evaluation of Tweedie exponential dispersion model densities. Statistics and Computing 15:267-280. https://doi.org/10.1007/s11222-005-4070-y
Einarsson Á, Stefánsdóttir G, Jóhannesson H, Ólafsson JS, Gíslason GM, Wakana I, Gudbergsson G, Gardarsson A (2004) The ecology of Lake Myvatn and the River Laxá: Variation in space and time. Aquat Ecol 38:317-348. https://doi.org/10.1023/B:AECO.0000032090.72702.a9
Elliott JM Baroudy E (1995) The ecology of Arctic charr, *Salvelinus alpinus*, and brown trout, *Salmo trutta*, in Windermere (northwest England). Nord J Freshwat Res 71:33-48.
Enevoldsen J, Simpson GL, Vistisen ST (2022) Using generalized additive models to decompose time series and waveforms, and dissect heart–lung interaction physiology. Journal of Clinical Monitoring and Computing 37:165-177. https://doi.org/10.1007/s10877-022-00873-7
Gallagher BK Fraser DJ (2024) Stream groundwater inputs generate fine-scale variation in brook trout phenology and growth across a warming landscape. Freshwat Biol 68:127-142. https://doi.org/10.1111/fwb.14198
Gebhardt A, Bivand R, Sinclair D (2024) interp: Interpolation Methods https://doi.org/10.32614/CRAN.package.interp
Ghinter L Youcef WA (2021) Local, seasonal, and yearly condition of juvenile Greenland halibut revealed by the Le Cren condition index. Trans Am Fish Soc 150:730-747. https://doi.org/10.1002/tafs.10324
Gibson JAE (1999) The meromictic lakes and stratified marine basins of the Vestfold Hills, East Antarctica. Antarct Sci 11:175-192. https://doi.org/10.1017/S0954102099000243
Gillis DP, Minns CK, Campana SE, Shuter BJ (2024) Major changes in fish thermal habitat diversity in Canadda's Arctic lakes due to climate change. Commun Earth Environ 5:89. https://doi.org/10.1038/s43247-024-01251-8
Gray E, Mackay EB, Elliott JA, Folkard AM, Jones ID (2020) Wide-spread incosistency in estimation of lake mixed depth impacts interpretation of limnological processes. Water Res 168:115136. https://doi.org/10.1016/j.watres.2019.115136
Gruber K Wieser W (1983) Energetics of development of the Alpine charr, *Salvelinus alpinus*, in relation to temperature and oxygen. J Comp Physiol, B 149:485-493. https://doi.org/10.1007/BF00690007
Haenel Q, Oke KB, Laurentino TG, Hendry AP, Berner D (2021) Clinal genomic analysis reveals strong reproductive isolation across a steep habitat transition in stickleback fish. Nature Communications 12:4850. https://doi.org/10.1038/s41467-021-25039-y
Holgerson MA, Richardson DC, Roith J, Bortolotti LE, Finlay K, Hornbach DJ, Gurung K, Ness A, Andersen MR, Bansal S, Finlay JC, Cianci-Gaskill JA, Hahn S, Janke BD, McDonald C, Mesman JP, North RL, Roberts CO, Sweetman JN, Webb JR (2022) Classifying mixing regimes in ponds and shallow lakes. Water Resources Research 58:e2022WR032522. https://doi.org/10.1029/2022WR032522
Hooker OE, Adams CE, Chaverie L (2023) Arctic charr phenotypic responses to abrupt generational scale temperature change: an insight into how cold-water fish could respond to extreme climatic events. Environ Biol Fishes 106:909-922. https://doi.org/10.1007/s10641-022-01363-0
Jeppesen E, Christoffersen KS, Rautio M, Lauridsen TL (2020) Ecology of Arctic lakes and ponds. In: D. N. Thomas (ed) Arctic Ecology. Wiley-Blackwell, Hoboken, NJ. https://doi.org/10.1002/9781118846582.ch7
Jónasson PM (1992) The ecosystem of Thingvallavatn: A synthesis. Oikos 64:405-434. https://doi.org/10.2307/3545062
Judson BJ, Kristjánsson BK, Leblanc CA-L, Ferguson MM (2024) The role of neutral and adaptive evolutionary processes on patterns of genetic diversity across small cave-dwelling populations of Icelandic Arctic charr (*Salvelinus alpinus*). Ecol Evol 14:e11363. https://doi.org/10.1002/ece3.11363
Kahilainen KK, Patterson WP, Sonninen E, Harrod C, Kiljunen M (2014) Adaptive radiation along a thermal gradient: Preliminary results of habitat use and respiration rate divergencce among whitefish morphs. PLoS ONE 9:e112085. https://doi.org/10.1371/journal.pone.0112085

Kavanagh KD, Haugen TO, Gregersen F, Jernevall J, Vøllestad LA (2010) Contemporary temperature-driven divergence in a Nordic freshwater fish under conditions commonly thought to hinder adaptation. BMC Evol Biol 10:350. https://doi.org/10.1186/1471-2148-10-350
Kelly S, Moore TN, Eyto Ad, Dillane M, Goulon C, Guillard J, Lasne E, McGinnity P, Poole R, Winfield IJ, Woolway RI, Jennings E (2020) Warming winters threaten peripheral Arctic charr populations of Europe. Clim Change 163:599-618. https://doi.org/10.1007/s10584-020-02887-z
Klemetsen A (2013) The most variable vertebrate on Earth. J Ichthyol/Vopr Ikhtiol 53:781-791. https://doi.org/10.1134/S0032945213100044
Kristjánsson BK, Combot D, Reilent A, Phillips JS, Leblanc CA-L (2024) Invertebrate diversity in groundwater-filled lava caves is influenced by both neutral- and niche-based processes. Ecol Evol 14:e11560. https://doi.org/10.1002/ece3.11560
Kristjánsson BK, Skúlason S, Snorrason SS, Noakes DLG (2012) Fine-scale parallel patterns in diversity of small benthic Arctic charr (*Salvelinus alpinus*) in relation to the ecology of lava/groundwater habitats. Ecol Evol 2:1099-1112. https://doi.org/10.1002/ece3.235
Le Cren ED (1951) The length-weight relationship and seasonal cycle in gonad weight and condition in the perch (*Perca flavescens*). J Anim Ecol 20:201-219. https://doi.org/10.2307/1540
Leblanc CA, Horri K, Skúlason D, Benhaim D (2019) Subtle temperature increase can interact with individual size and social context in shaping phenotypic traits of a coldwater fish. PLoS ONE 14:e0213061. https://doi.org/10.1371/journal.pone.0213061
Leblanc CA, Räsänen K, Morrissey M, Skúlason S, Ferguson M, Kristjánsson BK (2024) Fine scale diversity in the lava: genetic and phenotypic diversity in small populations of Arctic charr *Salvelinus alpinus*. BMC Ecology and Evolution 24:45. https://doi.org/10.1186/s12862-024-02232-3
Malmquist HJ, Ingimarsson F, Ingvason HR, Stefánsson SM, Hrafnsdóttir Þ (2020) Hlýnun Þingvallavatns og hitaferlar í vatninu. Náttúrufræðingurinn 90:80-99.
McDonald DG McMahon BR (1977) Respiratory development in Arctic charr *Salvelinus alpinus* under conditions of normoxia and chronic hypoxia. Can J Zool 55:1461-1467. https://doi.org/10.1139/z77-189
Mittell EA, Leblanc CA, Kristjánsson BK, Ferguson MM, Räsänen K, Morrissey MB (2025) Spatiatemporal variation in size-dependent growth rates in small isolated populations of Arctic charr (*Salvelinus alpinus*). Royal Society Open Science 12:241802. https://doi.org/10.1098/rsos.241802
Murdoch A, Dempson JB, Martin F, Power M (2015) Temperature-growth patterns of individually tagged anadromous Arctic charr *Salvelinus alpinus* in Ungava and Labrador, Canada. Ecol Freshwat Fish 24:193-203. https://doi.org/10.1111/eff.12133
Nishikawa C, Medeiros AS, Eamer J, Wolfe BB (2024) Responses of shallow subarctic ponds to a warming climate in the Anthropocene: a palaeolimnoogical perspective from the Hudson Bay Lowlands, Canada. Boreas. https://doi.org/10.1111/bor.12685
O'Gorman EJ, Ólafsson ÓP, Demars BOL, Friberg N, Guðbergsson G, Hannesdóttir ER, Jackson MC, Johansson LS, McLaughlin ÓB, Ólafsson JS, Woodward G, Gíslason GM (2016) Temperature effects on fish production across a natural thermal gradient. Global Change Biol 22:3206-3220. https://doi.org/10.1111/gcb.13233
Ohlberger J, Brännström Å, Dieckmann U (2013) Adaptive phenotypic diversification along a temperature-depth gradient. The American Naturalist 182:359-373. https://doi.org/10.1086/671169
Pinheiro J, Bates D, R Core Team (2023) nlme: Linear and nonlinear mixed effects models, https://CRAN.R-project.org/package=nlme
R Core Team (2025) R: A language and environment for statistical computing. R Foundation for Statistical Computing, Vienna, Austria. https://www.R-project.org/
Rabaey JS Cotner JB (2024) The influence of mixing on seasonal carbon dioxide and methane fluxes in ponds. Biogeochemistry 167:1297-1314. https://doi.org/10.1007/s10533-024-01167-7
Ramón CL, Priet-Mahéo MC, Rueda FJ, Andradóttir H (2020) Inflow dynamics in weakly stratified lakes subject to large Isopycnal displacements. Water Resources Research 56:e2019WR026578. https://doi.org/10.1029/2019WR026578
Rautio M, Dufresne F, Laurion I, Bonilla S, Vincent WF, Christoffersen KS (2011) Shallow freshwater ecosystems of the circumpolar Arctic. Ecoscience 18:204-222. https://doi.org/10.2980/18-3-3463
Rodrigues TH, Chapelsky AJ, Hrenchuk LE, Mushet GR, Chapman LJ, Blanchfield PJ (2022) Behavioural responses of a cold-water benthivore to loss of oxythermal habitat. Environ Biol Fishes 105:1489-1507. https://doi.org/10.1007/s10641-022-01335-4

Sanderson S, Beausoleil M-O, O'Dea RE, Wood ZT, Correa C, Frankel V, Gorné LD, Haines GE, Kinnison MT, Oke KB, Pelletier F, Pérez-Jvostov F, Reyes-Corral WD, Ritchot Y, Sorbara F, Gotanda KM, Hendry AP (2021) The pace of modern life, revisited. Mol Ecol 31:1028-1043. https://doi.org/10.1111/mec.16299

Seymour M, Räsänen K, Holderegger R, Kristjánsson BK (2013) Connectivity in a pond system influences migration and genetic structure in threespine stickleback. Ecol Evol 3:492-502. https://doi.org/10.1002/ece3.476

Simpson GL (2018) Modelling palaeoecological time series using generalised additive models. Frontiers in Ecology and Evolution 6:149. https://doi.org/10.3389/fevo.2018.00149

Smith SA Bella DA (1973) Dissolved oxygen and temperature in a stratified lake. Journal (Water Pollution Control Federation) 45:119-133.

Song K, Xenopoulos MA, Buttle JM, Marsalek J, Wagner ND, Pick FR, Frost PC (2013) Thermal stratification patterns in urban ponds and their relationships with vertical nutrient gradients. J Environ Manage 127:317-323. https://doi.org/10.1016/j.jenvman.2013.05.052

Thórarinsson S (1979) The postglacial history of the Mývatn area. Oikos 32:17-28. https://doi.org/10.2307/3544218

Verpoorter C, Kutser T, Seekell DA, Tranvik LJ (2014) A global inventory of lakes based on high-resolution satellite imagery. Geophys Res Lett 41:6396-6402. https://doi.org/10.1002/2014GL060641

Wagner DN, Baris TZ, Dayan DI, Du X, Oleksiak MF, Crawford DL (2017) Fine-scale genetic structure due to adaptive divergence among microhabitats. Heredity 118:594-604. https://doi.org/10.1038/hdy.2017.6

Wetzel RG (2001) Fate of Heat Limnology: Lake and river ecosystems. Academic Press, San Diego, Ca. pp 71-92,

Winslow L, Read J, Woolway R, Brentrup J, Leach T, Zwart J, Albers S, Collinge D (2019) rLakeAnalyzer: Lake physics tools https://doi.org/10.32614/CRAN.package.rLakeAnalyzer

Wood S (2023) mgcv: Mixed GAM Computation Vehicle with Automatic Smoothness Estimation. S. Wood, (ed), CRAN. cran.r-project.org/web/packages/mgcv/

Wood SN (2003) Thin Plate Regression Splines. Journal of the Royal Statistical Society: Series B (Methodological) 65:95-114. https://doi.org/10.1111/1467-9868.00374

Wood SN (2011) Fast stable restricted maximum likelihood and marginal likelihood estimation of semiparametric generalized linear models. Journal of the Royal Statistical Society: Series B (Methodological) 73:3-36. https://doi.org/10.1111/j.1467-9868.2010.00749.x

Wood SN (2017) Generalized Additive Models. Chapman and Hall/CRC, New York. https://doi.org/10.1201/9781315370279

Woolway RI, Sharma S, Smol JP (2022) Lakes in hot water: The impacts of a changing climate on aquatic ecosystems. Bioscience 72:1050-1061. https://doi.org/10.1093/biosci/biac052

Woolway RI, Sharma S, Weyhenmeyer GA, Debolskiy A, Golub M, Mercado-Bettín D, Perroud M, Stepanenko V, Tan Z, Grant L, Ladwig R, Mesman J, Moore TN, Shatwell T, Vanderkelen I, Austin JA, DeGasperi CL, Dokulil M, La Fuente S, Mackay EB, Schladow SG, Watanabe S, Marcé R, Pierson DC, Thiery W, Jennings E (2021) Phenological shifts in lake stratification under climate change. Nature Communications 12:2318. https://doi.org/10.1038/s41467-021-22657-4

Supplementary Tables

Supplementary Table 1. GAM Model Results for C23

Summary results for models except 2, seasonal, 2 – AR1, and seasonal – AR1, which are reported in Table 2. All GAMs were run using the Tweedie distribution with a log link function. None of the below models incorporate autoregressive components. As described in Table 1, models 1-6 have a 1-day lag on all independent variables, while models 7-12 use a 2-day lag. The wind direction spline is cyclic such that values of 0 and 360 are equivalent.

Model	Terms	Spline/ Smooth Type	edf	F	p	
1	T	TPRS	3.39	22.03	<0.001	***
	W_d	Cyclic	3.25	2.38	<0.001	***
3	T	TPRS	2.91	28.78	<0.001	***
	W_d	Cyclic	1.52	1.62	0.033	*
	W_s	TPRS	1.079	9.23	0.003	**
	W_dW_s	Cyclic:TPRS	2.37	0.72	0.009	**
4	T	TPRS	2.76	31.01	<0.001	***
	W_d	Cyclic	1.49	1.37	0.054	
	W_s	TPRS	1.98	4.79	0.008	**
	TW_dW_s	TPRS: Cyclic:TPRS	1.30	0.06	0.110	
5	T	TPRS	2.92	26.06	<0.001	***
	W_d	Cyclic	2.50	6.51	<0.001	***
	TW_dW_s	TPRS: Cyclic:TPRS	0.52	0.01	0.270	
6	T	TPRS	2.64	33.29	<0.001	***
	W_d	Cyclic	1.40	1.39	0.041	*
	W_s	TPRS	1.00	9.49	0.003	**
	W_dW_s	Cyclic:TPRS	2.54	0.88	0.004	**
	TW_dW_s	TPRS: Cyclic:TPRS	1.94	0.05	0.228	
7	T	TPRS	2.93	22.88	<0.001	***
	W_d	Cyclic	1.06	0.25	0.128	
8	T	TPRS	2.92	24.90	<0.001	***
	W_d	Cyclic	0.78	0.45	0.152	
	W_dW_s	Cyclic:TPRS	2.44	0.37	0.095	
9	T	TPRS	2.85	27.85	<0.001	***
	W_d	Cyclic	0.45	0.19	0.250	
	W_s	TPRS	1.00	0.48	0.491	
	W_dW_s	Cyclic:TPRS	2.62	0.45	0.062	
10	T	TPRS	2.58	40.63	<0.001	***
	W_d	Cyclic	1.8×10^{-5}	0.00	0.388	
	W_s	TPRS	1.00	0.65	0.423	
	TW_dW_s	TPRS: Cyclic:TPRS	2.04	0.15	0.014	*
11	T	TPRS	2.63	36.76	<0.001	***
	W_d	Cyclic	0.34	0.14	0.265	
	TW_dW_s	TPRS: Cyclic:TPRS	1.98	0.14	0.017	*
12	T	TPRS	2.48	43.11	<0.001	***
	W_d	Cyclic	3.4×10^{-5}	0.00	0.412	
	W_s	TPRS	1.00	0.97	0.328	
	W_dW_s	Cyclic:TPRS	1.42	0.20	0.153	
	TW_dW_s	TPRS: Cyclic:TPRS	1.91	0.12	0.028	*

Supplementary Figures

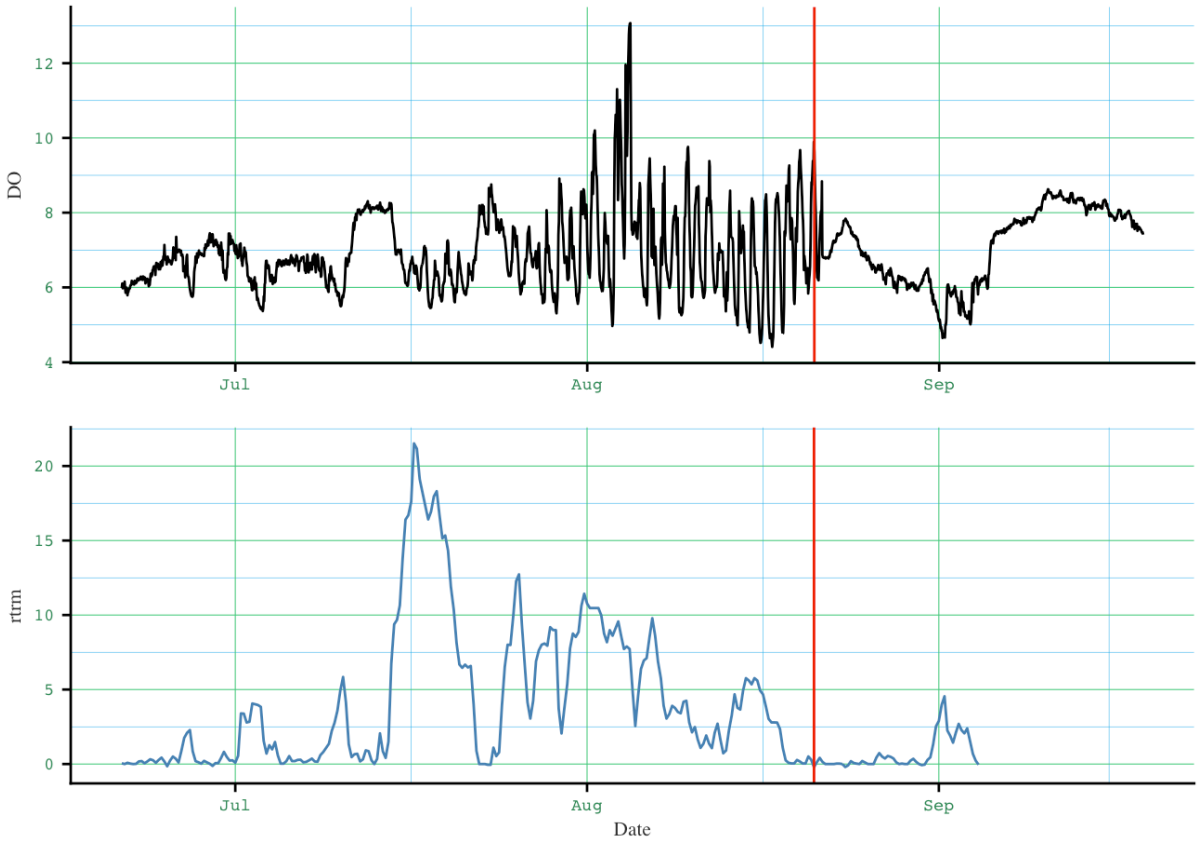

Figure S1. DO Concentrations (mgL^{-1}) and RTRM in C23
Full DO concentration recordings from MiniDOT logger, and RTRM. Vertical line indicates when the logger was removed and then replaced so the pond could be electrofished.

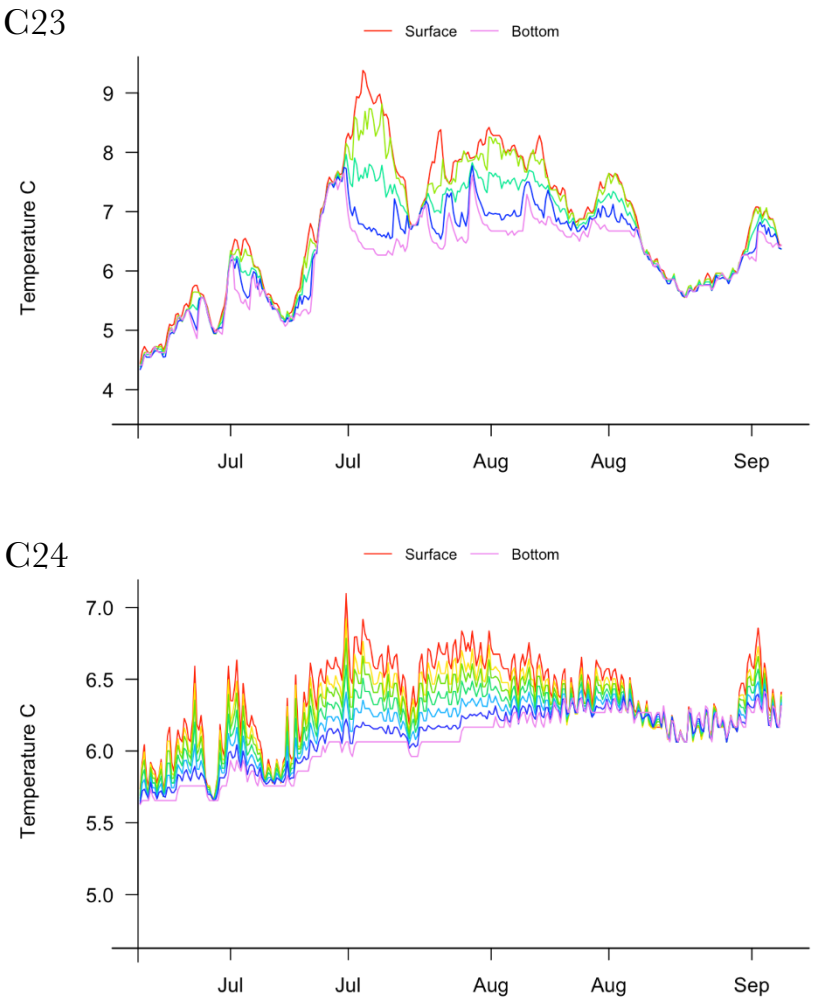

Figure S2. Thermal Profiles by Logger
Thermal profiles are shown with color gradient indicating logger depth, with loggers separated by 20 cm. The data presented here is the same as the data presented in Figure 1, but visualized in a way that emphasizes temperature differences between depths.

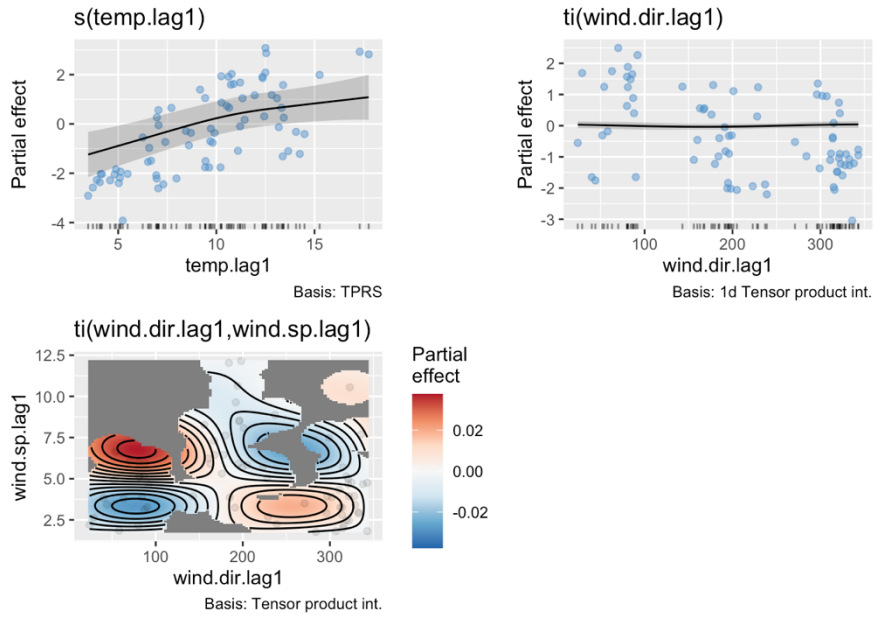

Figure S3. Partial Effects of GAM 2–AR1
Partial effects of GAM model 2–AR1. Of these effects, only *temperature* is significant, when the AR1 correlation structure is included in the model.

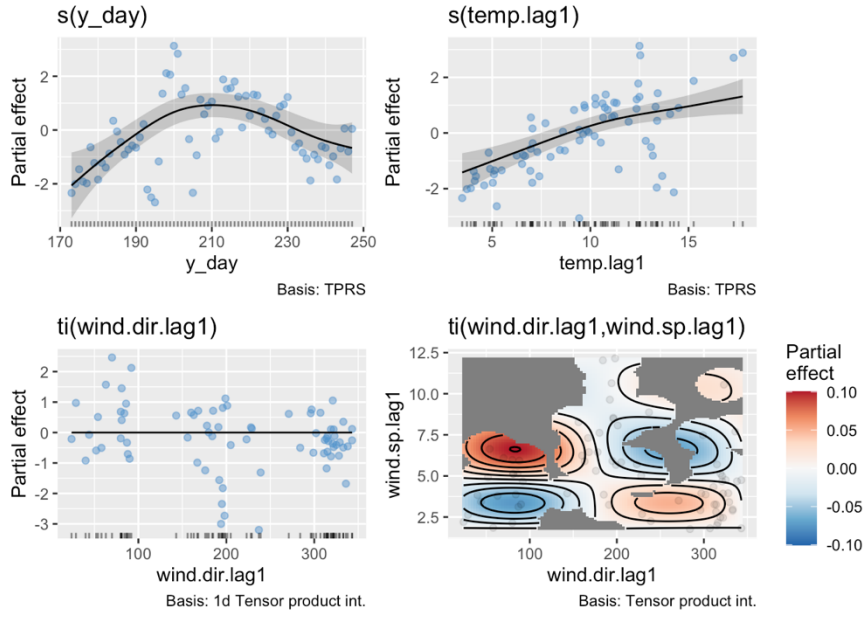

Figure S4. Partial Effects of GAM Seasonal–AR1
Partial effects of GAM model Seasonal–AR1. All are main effects are significant, when the AR1 correlation structure is included in the model.

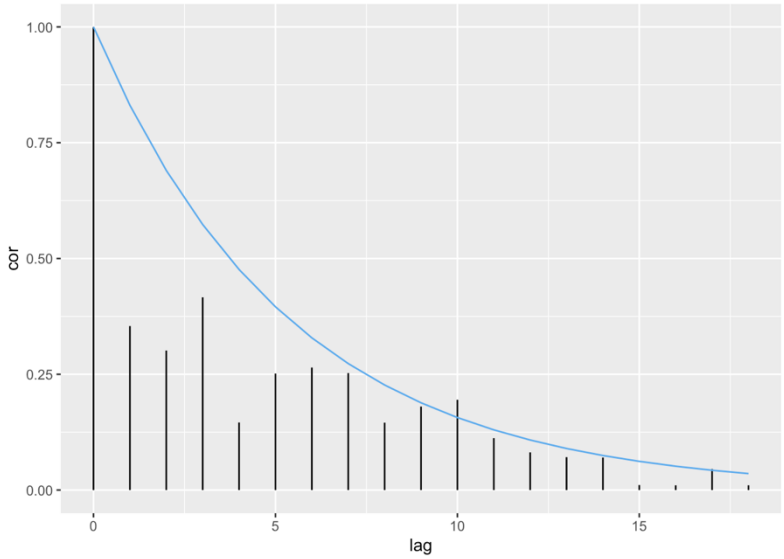

Figure S5. Model 2 Residual Autocorrelation
Vertical bars are an ACF plot of GAM model 2 residuals, showing clear autocorrelation. Blue curve shows exponential decay in temporal autocorrelation, using autocorrelation coefficient obtained by *gamm()* model with first-order autoregressive correlation structure, as described in supplementary methods.

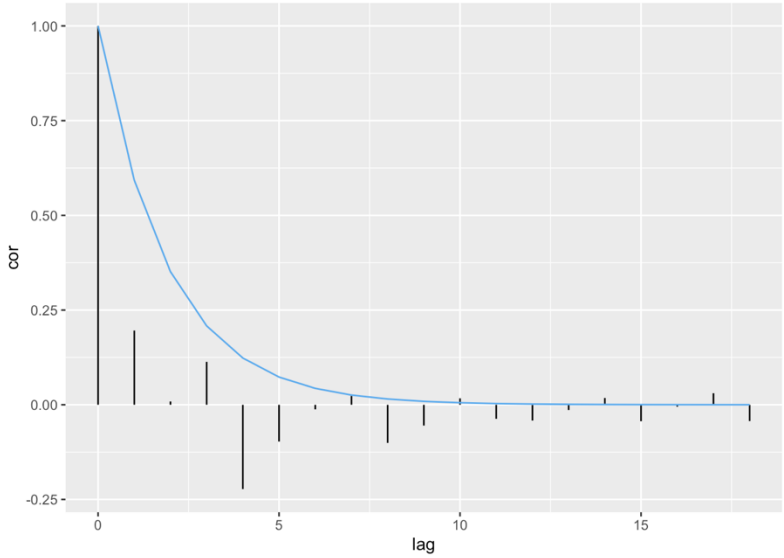

Figure S6. Seasonal Model Residual Autocorrelation
Vertical bars are an ACF plot of Seasonal GAM model residuals, showing clear autocorrelation. Blue curve shows exponential decay in temporal autocorrelation, using autocorrelation coefficient obtained by *gamm()* model with first-order autoregressive correlation structure, as described in supplementary methods.

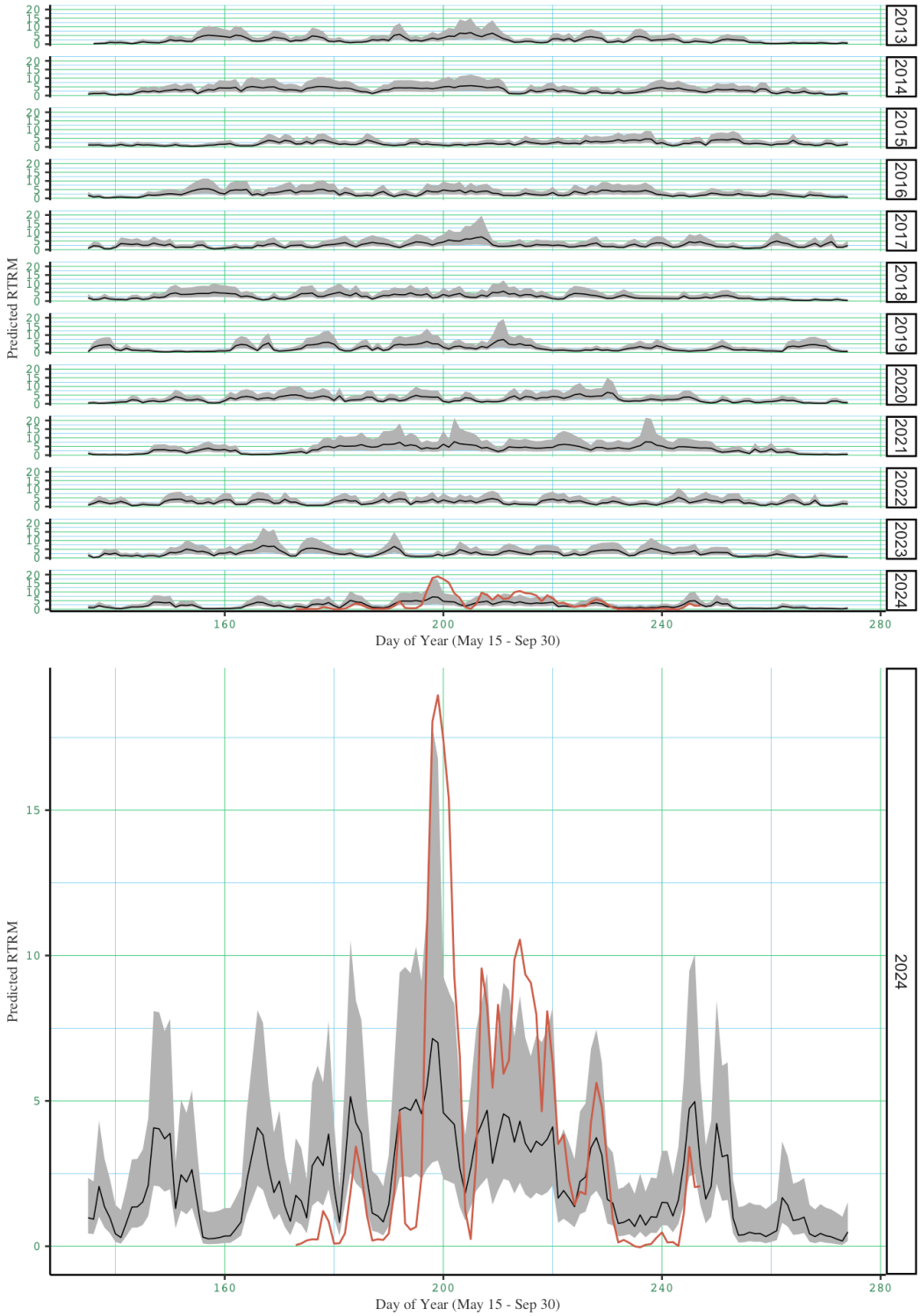

Figure S7. Hindcast Using Model 2–AR1 and Meteorological Data
Figure shows Model 2–AR1 fitted values of RTRM using historical meteorological data for May 15-September 30 in 2013-2024 (top panel) and 2024 only (bottom panel). Orange lines in 2024 represent measured daily average RTRM values. Grey bands represent 95% credible interval

around fitted values. This model includes an AR1 correlation structure, and thus incorporates autoregressive effects.

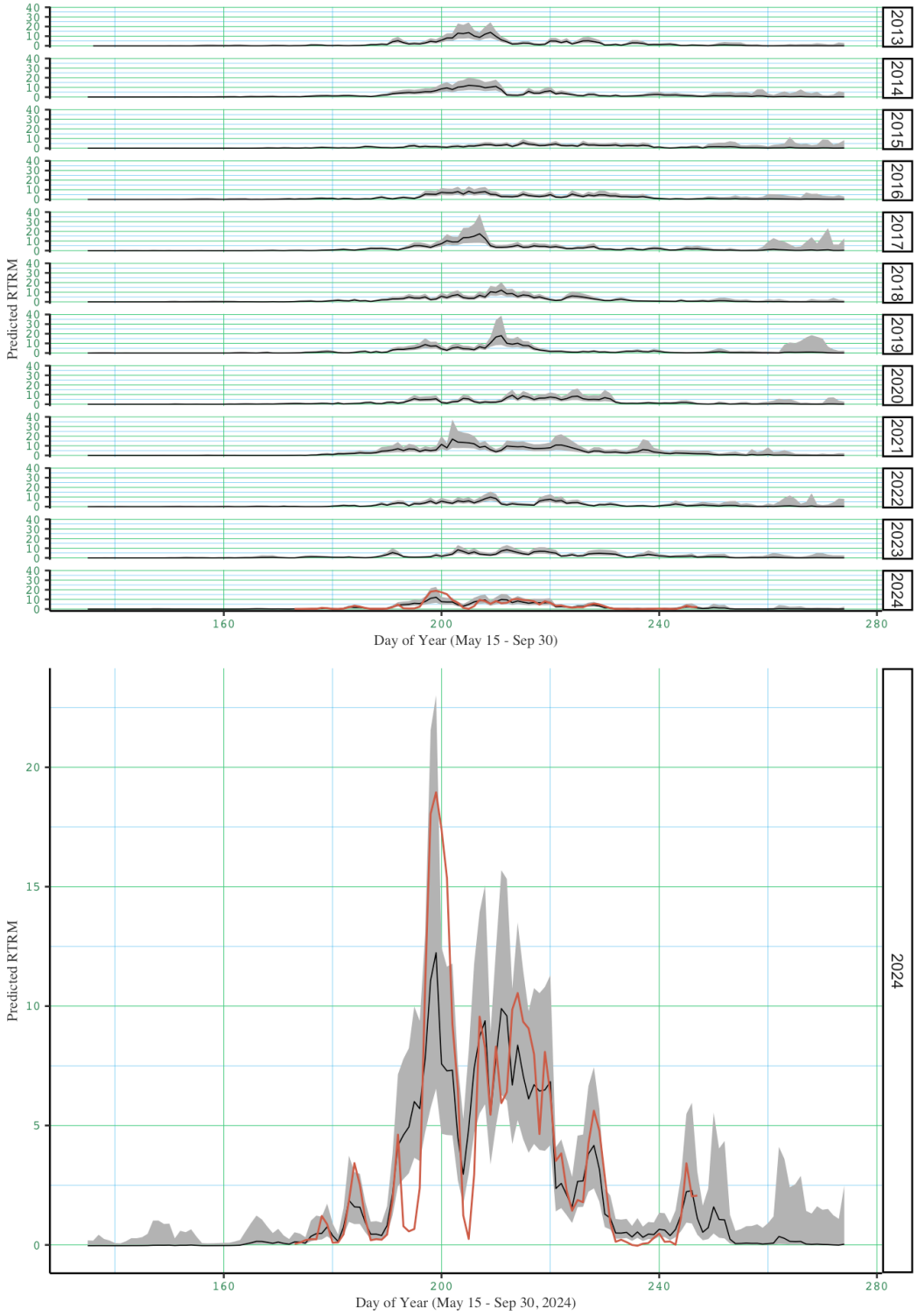

Figure S8. Hindcast Using Model Seasonal–AR1 and Meteorological Data

Figure shows model Seasonal–AR1 fitted values of RTRM using historical meteorological data for May 15-September 30 in 2013-2024 (top panel) and 2024 only (bottom panel). Orange lines in 2024 represent measured daily average RTRM values. Grey bands represent 95% credible interval around fitted values. This model includes a *day* term and AR1 correlation structure, and thus incorporates seasonal and autoregressive effects.

Supplementary Methods

The appropriate distribution and link function for the GAMs used to model RTRM in C23 is somewhat difficult to determine because of the unusual characteristics of RTRM as a variable. Because the variance of RTRM increases with its value, it is heteroscedastic, but it is also not bounded by zero. Instead, RTRM values below 0 are possible, but unstable, because they indicate upper layers of water that are more dense that lower layers. This means that RTRM has a functional limit slightly below zero, and can dip into negative numbers on cool summer days (or more rarely on winter days when air temperatures are between 0° and 4°). We resolved this issue by modeling GAMs using Tweedie distributions with a log link function, and added the absolute value of the minimum RTRM to make all response values ≥ 0. Where possible, the Tweedie distribution family was modeled using *mgcv*'s *tw()* function, which automatically fits its own *p* parameter. However, while *tw()* is available for *gam()* and *bam()* models, it is not available in *gamm()*, which was used to determine autocorrelation coefficients as described below. In *gamm()* models we used *Tweedie()* for the model family and supplied the value for *p* returned in the output of non-autoregressive models.

Although estimates of autocorrelation coefficients can be obtained from autocorrelation functions (ACF) on model residuals, as in Enevoldsen et al. (2022), they can also be identified using general additive mixed models (GAMMs) with autoregressive correlation structures, as in Simpson (2018). In our models, the autocorrelation coefficients returned by GAMMs were substantially higher than those implied by ACFs (see Figures S5 and S6), presumably because the AR1 correlation structures absorbed some of the variance that was partitioned to the independent variables in non-autoregressive GAMs. We then used the correlation coefficients return by the GAMMs as the input rho value in an analogous *bam()* model, which can use the more flexible *tw()* function to model the distribution family. Because the autocorrelation coefficients are so high, the autoregressive models we report should be taken extremely cautiously, particularly because our independent variables are meteorological in nature, and therefore also temporally autocorrelated.